ABSTRACT

CHEMISTRY

IKPONMWEN, FRANK O. B.Sc. UNIVERSITY AT BUFFALO, 2011

PREPARATION OF MAGNESIUM-ALUMINUM LAYERED DOUBLE HYDROXIDES (MgAl-LDH) AND DETERMINATION OF THE QUANTUM EFFICIENCY OF CsSb PHOTOCATHODE ON DIFFERENT SUBSTRATES

Committee Chair: Ishrat Khan, Ph.D.

Dissertation dated May 2020

This dissertation consists of two parts. The first focuses on the synthesis and characterization of Mg^{2+}/Al^{3+}-LDH-DS/$S_2O_8^{2+}$-•H_2O/C_3H_6OH. The second focuses on the growth and spectral response of CsSb photocathode(s) on Si, Al_2O_3, TiO_2, and SiC. Layered double hydroxides ($[M^{II}_{1-x} M^{III}_{x} (OH)_2] (A^{n-})_{x/m} \cdot nH_2O$) are layered materials known as anionic clays, or hydrotalcite-like compounds started in the early 1980s, has become a class of layered materials having projections and promise in the field of biomaterials, drug delivery, sensors, molecular and imprinting. In this investigation, we approached a method to identify counterfeit drugs in a well-controlled environment, which is an approach that will be cheaper and conducive to society. There are two significant steps in accomplishing this investigation. The first, which is discussed in this project, is intercalating Mg^{2+}/Al^{3+}-LDH-DS/$S_2O_8^{2+}$-•H_2O/C_3H_6OH in distinct layers that will be inducive for polymerization. One of the significant accomplishments has been to

intercalate both sodium dodecyl sulfate and persulfate ions between the layers and for the adsorption of allyl alcohol. We began with synthesizing Mg^{2+}/Al^{3+}-LDH-NO_3 with a d-spacing of 7.88Å. The layers increased to 35.9Å when replaced by Mg^{2+}/Al^{3+}-LDH-DS. These preliminary results validate our approach and open the way to developing imprinted polymers that can identify counterfeit drugs.

The second part focuses on the growth and spectral response of CsSb photocathodes on Si, Al_2O_3, TiO_2, and SiC. Alkali antimonides are efficient photocathode materials due to their high quantum efficiency compared to other materials. For this reason, a developed technique to better understand the growth and characterization of this material on different substrates. The growth of CsSb photocathodes is dependent on temperature, pressure, and deposition rate to obtain a better quantum efficiency (QE). The drive of this investigation was to explore the growth and spectral response of CsSb photocathodes on Si, Al_2O_3, TiO_2, and SiC along with their corresponding quantum efficiency. The growth thickness was measured using a quartz crystal microbalance (QCB). The results lead to the conclusion that SiC has a QE of 9.7%, which is an improvement compared to Si, Al_2O_3, TiO_2 - because SiC forms a better interface with Cs_3Sb because it does not contain oxygen.

PREPARATION OF MAGNESIUM-ALUMINUM LAYERED DOUBLE HYDROXIDES (MgAl-LDH) AND DETERMINATION OF THE QUANTUM EFFICIENCY OF CsSb PHOTOCATHODE ON DIFFERENT SUBSTRATES

A DISSERTATION

SUBMITTED TO THE FACULTY OF CLARK ATLANTA UNIVERSITY

IN PARTIAL FULFILLMENT OF THE REQUIREMENTS FOR

THE DEGREE OF DOCTOR OF PHILOSOPHY

BY

FRANK OSAZUWA IKPONMWEN

DEPARTMENT OF CHEMISTRY

ATLANTA, GEORGIA

MAY 2020

© 2020

FRANK OSAZUWA IKPONMWEN

All Rights Reserved

ACKNOWLEDGEMENTS

First, I thank God for good health through the years and the grace to complete this project. I remembered days before moving to Atlanta; I experienced the worst accident that almost cost my life. Today, I am here writing my doctoral dissertation. I want to use this platform to express my gratitude to my advisors, Dr. James Reed, Dr. Ishrat Khan, Dr. Issifu Harruna, and Dr. Xiao-Qian Wang, for their support over the years through this journey.

Besides my advisors, I also want to thank my committee members, Dr. Xiu-Ren Bu and Dr. Dinadayalane Tandabany, for their encouragement and support. I also want to thank my advisors from Cornell University, Dr. Ivan Bazarov, Dr. Ritchie Patterson, Dr. Luca Cultrera, and Dr. Alice Galdi, who gave me the opportunity and introduced me to photocathode. This work is supported by Title III, NSF/CREST/CFNM Award #HRD-1137751, and NSF Physics Grant #1549132.

Lastly, I want to thank my family, Godwin Ikponmwen, Sussiana Ikponmwen, Agharese Ikponmwen, Obinna Obianom, Marvelous Ikponmwen, Adesuwa Ikponmwen, Osaro Ikponmwen, Asana Aruna, Feyitoluwa Tola-Adelani, and Linda Ikponmwen for their support throughout my Ph.D. journey. I dedicate this dissertation to my family, my wife, my friends, and everyone for their constant support and unconditional love.

TABLE OF CONTENTS

CHAPTER

CHAPTER

LIST OF FIGURES

Figure

Figure

LIST OF TABLES

Table

LIST OF ABBREVIATIONS

Keywords:

MIPs	Molecularly Imprinted Polymers
LDHs	Layered Double Hydroxide
MIT	Molecular Imprinting Technology
SDS	Sodium Dodecyl Sulfate
DS	Dodecyl Sulfate
TGA	Thermogravimetric Analysis
SEM	Scanning Electron Microscope
FTIR	Fourier-Transform Infrared Spectroscopy
XRD	X-Ray Diffraction
PXRD	Powder X-Ray Diffraction
Si	Silicon
SiC	Silicon Carbide
Al_2O_3	Aluminum Oxide
TiO_2	Titanium Dioxide

CHAPTER 1

LAYERED DOUBLE HYDROXIDES

1.1 Introduction of Layered Double Hydroxides

The need to identify counterfeit drugs effectively and inexpensively has a higher demand now than ever before, especially today in the 21st century, where the use of technology has advanced our knowledge and expanded our ideas. These ideas developed considering economically underdeveloped countries that do not have the equipment and resources to carry out counterfeit drug testing. For example, people have died and have injured as a result of taking fake or counterfeit drugs. They were taking different types of medications without labels, and the ones with the name were wrong when purchased, leading to more and several medical attentions.

According to the World Health Organization (WHO), "almost half of the counterfeit drugs and low-quality drugs reported between 2013 and 2017 were found to be in sub-Saharan Africa, costing about $200 billion worldwide.[1] One of the significant reported reasons why the general public buys these drugs due to the high price for the brand name drugs that people could not afford, and they instead settle for the ones sold on the street. They believed the solution to their problem has been to find these medications on the street for a lower and reasonable price. The belief has been that the drugs would not harm them. All this has contributed to the idea and needs to identify counterfeit drugs inexpensively so that low-income families can carry out these tests.

The danger will continue to increase, and more lives will be affected as a result of people taking fake or counterfeit drugs available in low-income countries. According to the World Health Organization (WHO), it says:

> A WHO report shows that Africa alone accounts for 42% of the global cases of substandard and fake medical products. The United Nations (UN) Office on Drug and Crime suggests that the penetration of counterfeit pharmaceuticals has been much higher in the developing world, reaching 30%, as opposed to less than 1% in the developed world. Perpetrators of the phenomenon see Africa as a soft target because the continent has weak technical capacity and tools when compared with the West.[2]

This is a huge number compared to the developed nations, with only 1% of the people taking fake or counterfeit drugs. There is a need to find a way to reduce the number from 30%, and it is the reason for this investigation.

The WHO also reported that "Analytical devices used to detect fake drugs are very expensive for widespread use in many African countries, costing between $45,000 and $67,000, and mostly imported. The hurdle is high and complicated by an absence of systemized collection of data on counterfeit and substandard medicines on the continent".[2] This work will be a straightforward method used in schools and third-world countries, which are not capable of purchasing high-performance liquid chromatography or gas chromatography instruments. The ultimate goal of this work is to be able to identify counterfeit drugs cheaply and effectively. The goal is to develop an efficient and

inexpensive means to identify molecules using imprinted polymers. There is a need for an inexpensive means of identifying and separating a specific molecule in the presence of a large number of other molecules. There have been previous attempts to do this. The results have been unsatisfactory. Accomplishing this goal requires two parts, the first is to prepare layered double hydroxides (Mg^{2+}/Al^{3+}-LDH) with a well-structured environment. The second part is to carry out molecular imprinting successfully in these environments. Molecular imprinting is carried out via polymerization inside the LDH galleries using a template to imprint a specific molecule. The overall final goal will be to develop the ability to identify fake and counterfeit drugs sold anywhere in the world. The immediate goal of this dissertation is to provide proof-of-concept by demonstrating that the essential components of LDH nanoreactors fabricated. Preparation of designer polymers and carrying out polymerizations in well-controlled environments.

1.2 Project Rationale

The rationale for this project is that improved polymers prepared by carrying out the polymerizations in the customized environments of nanoscale mini reactors. The proposed mini reactors are the galleries of modified layered double hydroxides. The schematic diagram below (Figure 1) illustrates a current method for preparing molecular templates. The polymerization process requires a template of the desired molecule, a suitable solvent, a cross-linker, one or more functional monomers and an initiator.[3] The template must be compatible with the chosen functional monomer(s) because the success

of the polymerization is due to the template-monomer interaction. The polymerization carried out in the presence of the functional monomer(s). After the polymerization is complete, the template is extracted using a solvent, thus leaving only the templated polymer matrix behind.[4] The polymer matrix will have binding sites that have the shape and size that will bind the template used during the polymerization. The resulting polymer matrix will then recognize and bind to the target molecule. An additional requirement is that, if another molecule placed into the polymer matrix, it will not fit into or bind to the polymer matrix.

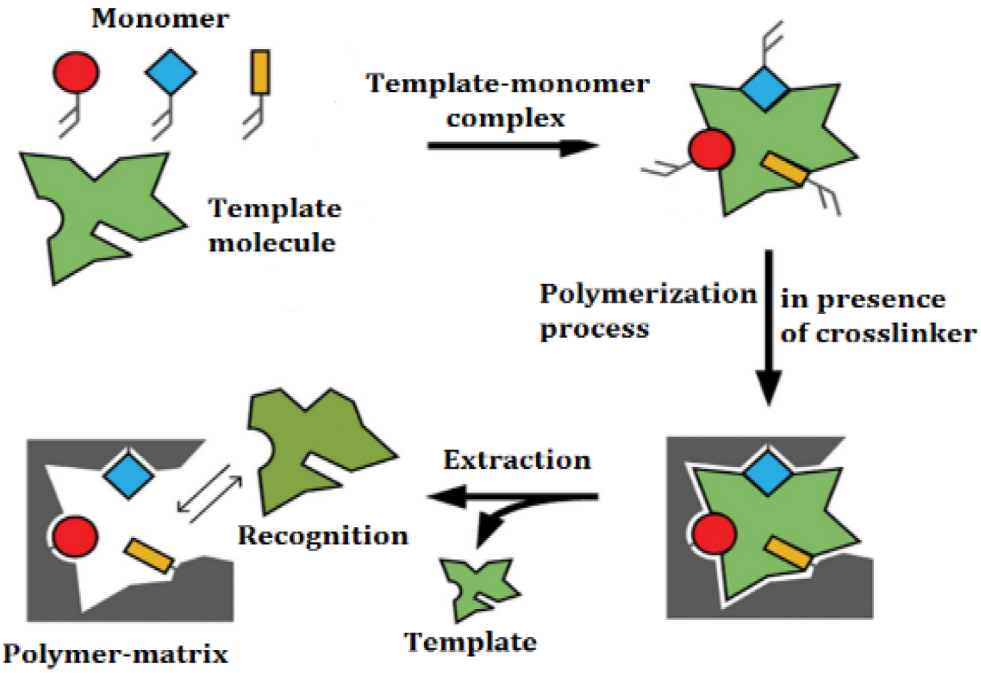

Figure 1. Scheme of molecular imprinting.[4]

In other to improve the quality of the templated polymers, it is proposed that the polymerizations carried out in the galleries of modified layered double hydroxides. Magnesium-aluminum layered double hydroxides (Mg^{2+}/Al^{3+}-LDH) are a class of metal hydroxides derived from the brucite structure (Figure 2).[5,6] Study of M^{2+}/M^{3+}-LDHs started in the mid-1900s due to their multiple applications in new polymer nanocomposites, ion exchange, photochemistry, drug delivery, catalysis and most importantly as mini-receptors for poymerization.[7-11] In addition, other critical applications include catalyst supports, controlled release of anions and photoactive materials.[12-15] The brucite structure is that of $Mg(OH)_2$, and due to its ionic radius and low electronegativity Mg^{2+} prefers to be surrounded by six oxygen atoms.[16-20]

The LDH galleries can be used as a mini reactor for the polymerization to take place. The most straightforward illustration to explain this is to imagine a building surrounded by walls. Imagine carrying out a task inside the building without the effect of the outside environment playing a factor in determining the outcome of the result. The building in this example corresponds to one gallery between the layers of the DH, which are composed of many layers stacked together. Everything within the building is suited for the task to be carried out successfully without the effect of the outside environment. Similarly, the role of LDH galleries is that of a mini reactor, in which the polymerization takes place.[21-24] This new technique hopes to improve the synthesis and effectiveness of molecular imprinting in identifying specific molecules.

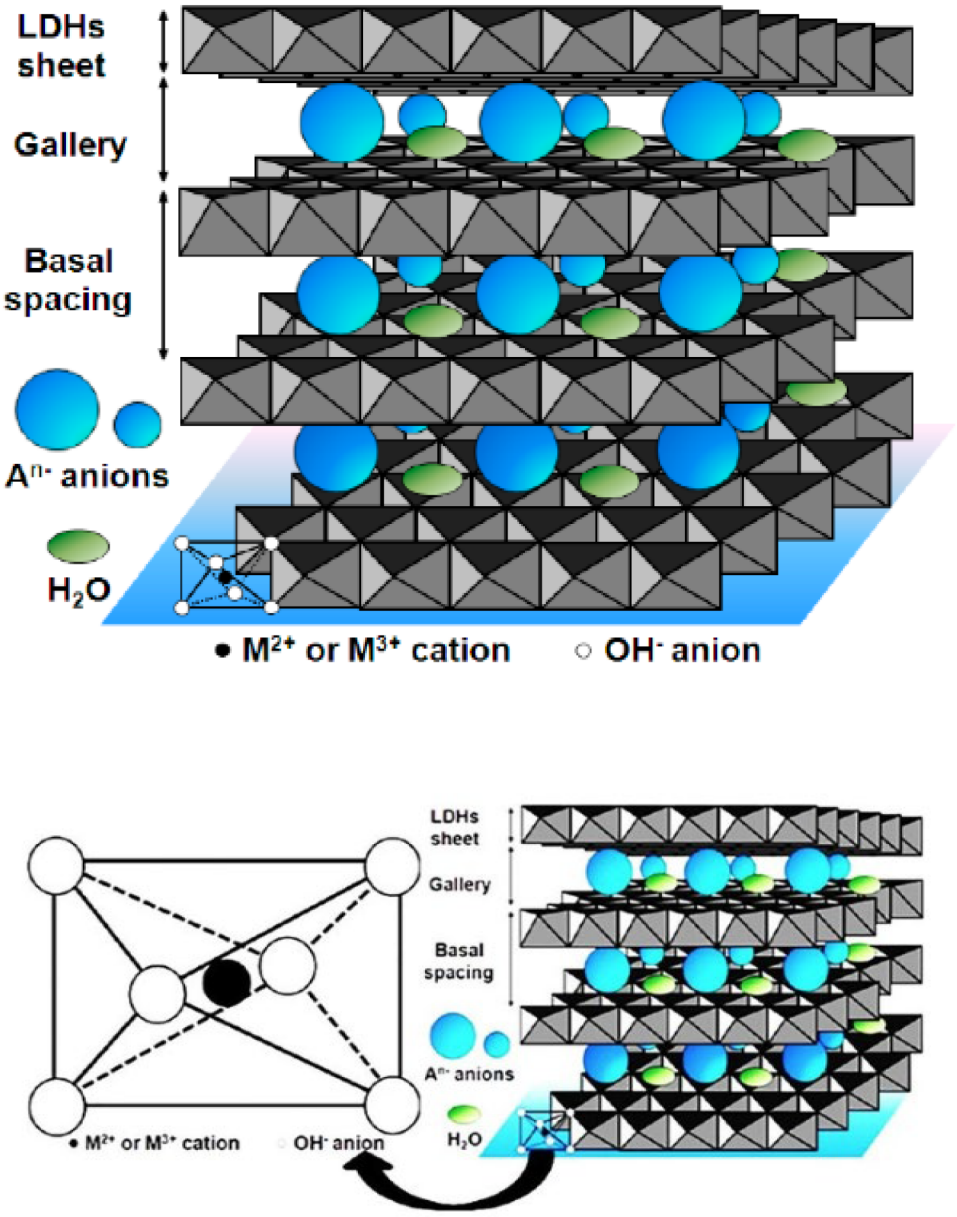

Figure 2. Schematic structure of layered double hydroxides (LDHs).[15]

1.3 Literature

1.3.1 Structure and Derived Properties of LDHs

Layered double hydroxides (LDHs) are hydrotalcite-like compounds discovered in the mid-19th century, which can be represented by the general formula $[M^{II}_{1-x} M^{III}_{x} (OH)_2] (A^{n-})_{x/m} \cdot nH_2O$.[25-27] The LDH structure derives from the brucite structure, which contains electrically neutral $M^{(2+)}(OH)_2$ layers. Replacement of some of the divalent metal ions in the layers by trivalent ions places a net positive charge on each layer $[M_{1-x}^{(2+)}M^{(3+)}_x(OH)_2]^{x+}$, where M^{2+} are divalent metal ions like Mg^{2+}, Ca^{2+}, Zn^{2+}, and M^{3+} are trivalent metal ions like Al^{3+}, Cr^{3+}, Fe^{3+}, Co^{3+}. A^{n-} is an anion such as Cl^-, CO_3^{2-}, or NO_3^-. The variable x is a fixed-composition over a range of $0.2 \leq x \leq 0.33$. The exact formula was not published until 1915 by Manasse.[28]

Mg^{2+}/Al^{3+}-LDHs are minerals and synthetic materials with positively charged brucite type layers of mixed metals hydroxides.[29-31] A positive charge exists in mixed divalent and trivalent metal hydroxides, in which its's charge-balance retained by the presence of anions in the interlayer regions.[32] Interest in LDH chemistry increased in 1942 following the publication of a series of papers by Feitknecht on what he called "*double sheet structures*".[33] Exchangeable anions, located in the interlayer spaces, compensate for the positive charge of its brucite layers. The counterions found in the galleries between the LDH layers. There are layers of hydroxyl groups between the metals and the counter ions shown in Figure 3. The binding of the counterions is electrostatic, which readily is replaced by other negative ions.

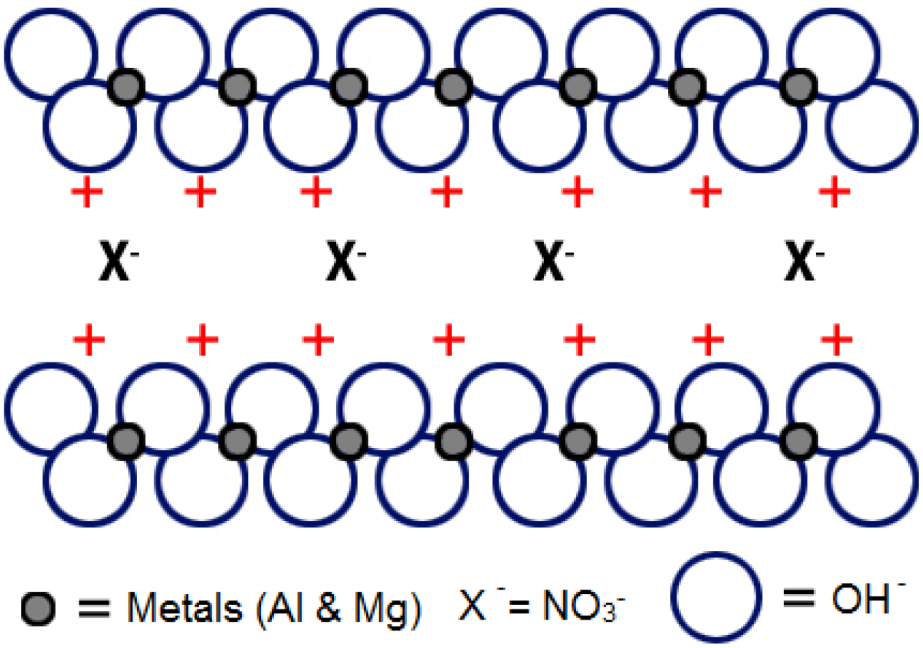

Figure 3. Schematic representation of the structure of layered double hydroxides.[34]

Different divalent and trivalent metal have been used in the LDHs synthesis and tend to have property differences. Using specific two or three elements together is they to achieve the best result due to the synergistic effect.[35] Also, alkaline metals tend, which are metal ions in group 2 (M^{+2}) chemically, form a structural LDH than transitional metals. In LDHs synthesis, four-layered double hydroxides of Cu-Zn-Cr, Zn-Cr, Ni-Al, and Cu-Ni-Cr showed high phosphate absorption capability.[35] However, most of the research and studies carried out have focused on using LDHs that consist of Mg and Al in their structure and nitrate ion in the LDH layers.[36-41] "To date, 44 minerals described as natural of LDH phases; commonly known to mineralogist as the 'hydrotalcite' or 'hydrotalcite group' of minerals".[42]

1.3.2 LDHs Morphologies

Many studies used LDHs for environmental purification, biomedical application, and as a catalyst by utilizing their intercalation properties.[42-44] LDHs generally have the hexagonal plate-shaped crystals stacked together, and the image of the nanoparticles obtained using the scanning electron microscope. Other research has shown that LDHs also have the spherical shape plate.[44] Establishing the guideline about morphological control can contribute to improving the properties of LDH materials.[45]

1.3.3 Powder X-ray Diffraction Studies

Powder x-ray diffraction (PXRD) is a scientific technique that uses x-ray diffraction on powder samples to identify the structure, basal spacing, crystallinity, including crystalline or amorphous of the material. These powder x-ray diffraction studies have been a technique that has been implemented years ago in identifying nanoparticles materials. The internal structure of the layers produces reflection at a point when the x-ray hits the sample. These reflections are in sequence of the basal spacing between the layers when the x-ray hits the sample.[44]The anions affect the size of the LDHs galleries of the shape of the anions. Among the anions found in the LDH galleries are Cl^-, Br^-, NO_3^-, CO_3^{2-}, SO_4^{2-}, and SeO_4^{2-}.[5,7] These anions can expand the layers of the LDH galleries leading to their having different basal. Some anions are easy to intercalate into the LDH layers, while some are hard and difficult to intercalate into the LDH layers.[7]

1.3.4 Relative Affinities of the Ions

The relative affinities for each anion are different, especially for the case of carbonate ion. LDHs resulted from carbonate contamination caused by CO_2 in the air during the preparation. Carbonate ion inside the LDHs contributes to the LDH shapes characterized using scanning electron microscopy (SEM), and also makes it challenging to intercalate other anions into the LDH layers. Naturally occurring Mg^{2+}/Al^{3+}-LDH can have rhombohedral and hexagonal structures, and these structures influenced by the presence of carbonate ion between the layers.[46,47] Mg^{2+}/Al^{3+}-LDH syntheses carried out under nitrogen gas, because of the high affinity resulting from the di-positive charge on carbonate ion.

Due to its ability to hydrogen bond and its geometry, carbon ion tends to bind very strongly to Mg^{2+}/Al^{3+}-LDH, and it is virtually impossible to remove it, making it difficult for any anion exchange to occur. Two major rules determine the relative affinities of ions for the functional group. The first rule is that ions with higher charge tend to have higher affinity (e.g., $Na^+ < Ca^{2+} < Al^{3+} < Cl^-$ and $< SO_4^{2-}$). The second rule is hat ion with the greatest size (radius) and the greatest charge has the highest affinity (e.g., $Li^+ < Na^+ < K^+ < Cs^+ < Mg^{2+} < Br^-$ and $< I^-$).

1.3.5 Co-intercalation Process

The word intercalation refers to a reversible inclusion or insertion of a molecule or an anion into the material between the layer's structures. The ions intercalated in the LDHs layers structure. Therefore, co-intercalation is the process where two ions placed into the structural layers of the material at the same time. For example, the most well-known case of co-intercalation is graphene, where both sodium and potassium are both co-intercalated for lithium-ion batteries.[48-49] The co-intercalation process showed a change in the nanoparticles when characterized by powder x-ray diffraction compare to when intercalated with just one ion. During co-intercalation, we tend to see an expansion of the structural layers to accommodation another ion. These changes reflect the increase in distance of the basal between the LDH layers. The morphology can also be proven using a scanning electron microscope if both ions were successfully co-intercalated into the LDH layers.[27,28]

1.3.6 Anion Exchange Process

Different anions exchanged in LDHs galleries. Among these are Cl^-, Br^-, NO_3^-, CO_3^{2-}, SO_4^{2-}, and SeO_4^{2-}. These anions can be complex and hard to exchange between the LDH layers. Generally, there are two different types of ion exchange carried out.[5] The first is the anion exchange, and the second is the cation exchange.[5] Generally, the ion exchange method in a cation such as Na^+, K^+, $ca^{+2,}$ and Mg^{+2} replaced by H^+ ion, reducing the pH of the solution. While anions such as Cl^-, F^-, Br^- and PO_4^{3-} are replaced by OH^- ions, therefore increasing the pH of the solution.[6]

Anion exchange used is carried out in chemical, petrochemical, pharmaceutical industries, including our household items. For example, ion exchange is an application used in high drinking water purification. The ion exchange method carried out with two different solutions, and the ion exchange takes place when both solutions are mixed. The ion exchange method was applied when carrying out the synthesis of Mg^{2+}/Al^{3+}-LDH NO_3. The exchange of two ions replacing LDH NO_3^- with dodecyl sulfate (DS) making LDH DS.

Ion exchange can impact the structure both positively and negatively. These impacts can contribute to the change of the structure of a crystalline or amorphous structure. LDHs studies have shown the corrected ions, and other ions have also intercalated into the LDH layers. The anions incorporated int the galleries in two different ways. [50] The first is the intercalation method, and the second is the exfoliated method shown in Figure 4. The intercalation method is a process where the LDHs are arranged in order and layers up together. The intercalation method is the most successful type of arrangement carried out with LDHs in polymerization. The produced from the LDHs polymerization produces nanocomposite consisting of the polymeric chain. The intercalation method often increased interlayer spacing. The other type is the exfoliation method, where the layers are all scattered, and no form of arrangement carried out.[50]

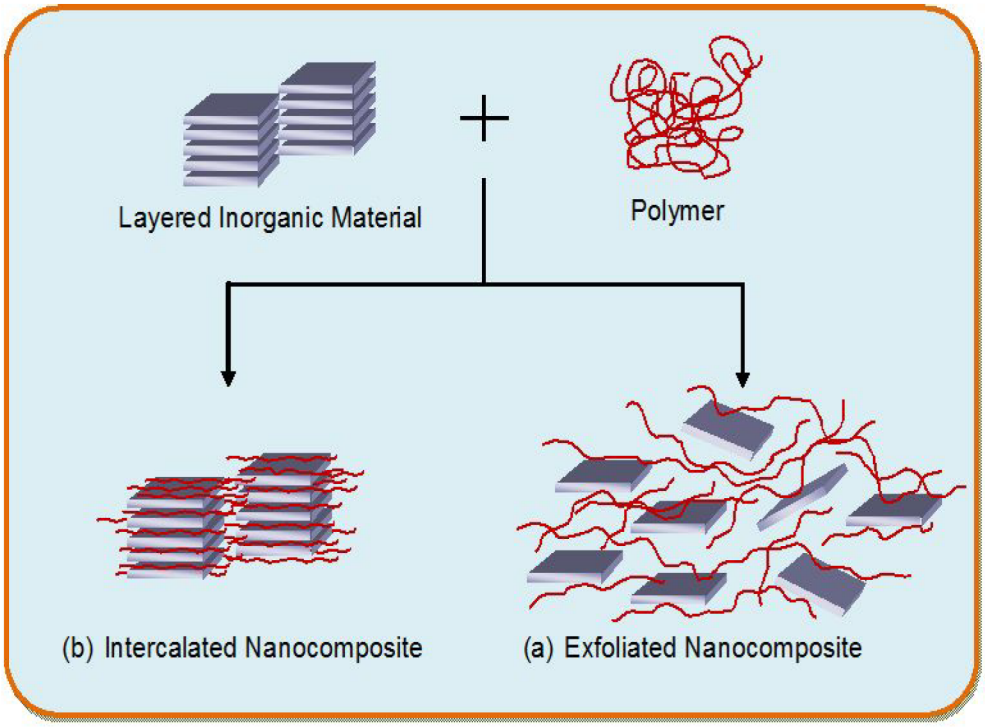

Figure 4. Schematic representation of the different types of composites. (a) Intercalation nanocomposite (b) Exfoliated nanocomposite.[50]

1.3.7 Polymerization

The mechanism for the free radical polymerization of olefins shown in Figure 5. The reaction begins with persulfate heated, which generates radical SO_4^{1-}. This reaction referred to as a free radical chain that requires a separate initiation step generated. Radical initiation reaction consists of two general types according to how the radical formed; these are the homolytic decomposition of covalent bonds by energy absorption, and the second is the electron transfer from one atom-containing unpaired electron.[51] One of the compelling methods of generating free radicals is vis low-temperature under mild condition, but the most effective method is redox initiation.[51] The condition to carry out

the bulk polymerization of the monomer of interest is to have a small amount of persulfate initiated into the LDH layers. This process accounts for creating more extended chain polymer and resulting in bulk polymerization. Actual polymerizations that have previously carried out in LDH galleries is vinyl alcohol.[52]

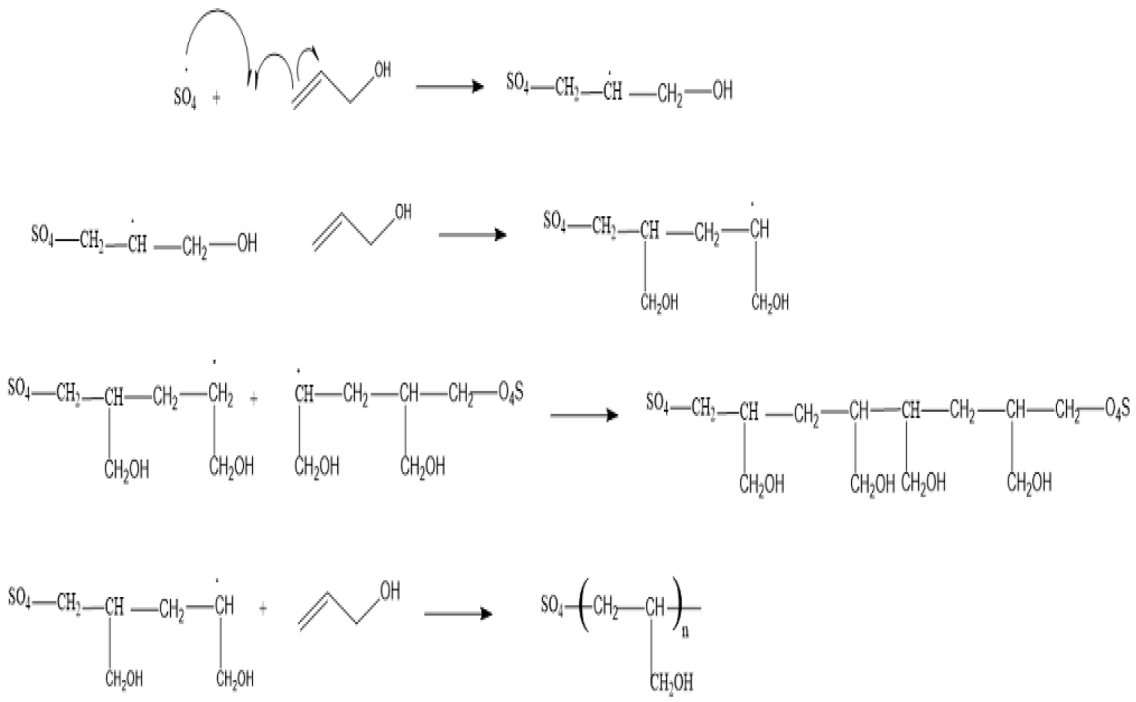

Figure 5. Example of radical polymerization using persulfate.

1.3.8 Molecular Imprinting

Molecular imprinting technology (MIT) has been one of the most effective and consistent methods for drug imprinting *via* polymerization.[53,54,55] Molecularly imprinted polymers (MIPs), obtained using the imprinting technology, are molecular recognition elements that can mimic natural recognition entities such as antibodies, catalysts, sensors, and biological receptors.[56,57,58] MIP's are useful in separating and analyzing complex biological fluids and various environmental samples.[59-63]

Molecular imprinting technology has long been introduced into the industry for years now as a simple, cheap and effective way to design molecular recognition, being able to mimic natural recognition entities such as antibodies, drugs, and biological receptor.[64-67] Molecular imprinting (MI) not only mimics drugs, but it has also frequently used for drug delivery. Molecularly imprinting started a long time ago by Polyakov in 1931 in his attempt to understand the principles underlying the adsorption properties and structure of silica gel in a range of applications.[68]

MI technology has also shown other promising prospect in other areas for the recognition in amino acids and proteins.[69-75] The polymerization requires several steps before being carried out. The most crucial step during the polymerization process is the first step; during this step, the process involves breaking of carbon-carbon double bond. The first step is generating the radical, and the second step is transferring radical from the initiator molecule to the monomer of interest. After the polymerization process, as illustrated in the schematic diagram in Figure 6, the desired template is removed from the polymer using solvent extraction. The polymer-matrix without the template will then

have its specific recognition site obtaining the shape, size, and binding sites to the template of interest. Thus, the resultant polymer matrix recognizes and binds selectively only to the templated molecules. This process is called a "lock and key" model. Several advantages of MI polymers shown in reviews with the capability of high selectivity and affinity for the target molecule used during polymerization.[76-79]

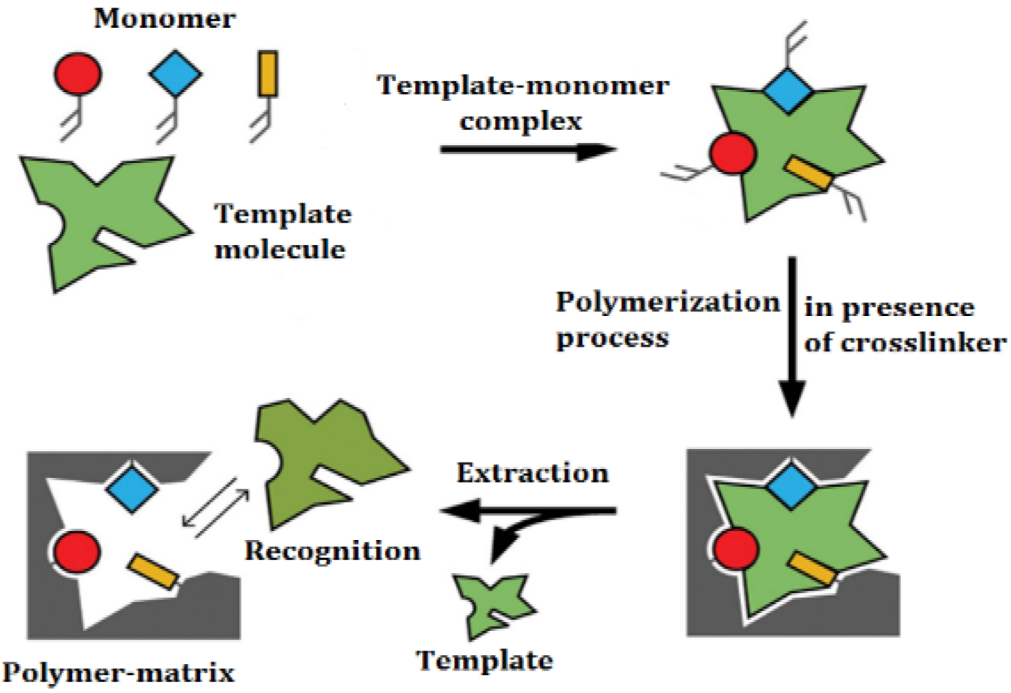

Figure 6. Polymerization process.[4]

After the polymer synthesis successfully carried out, the removal of the template molecules from the polymer via washing with solvent or the via extraction.[80] This process leaves binding sites that are complementary in shape to the template used shown in the literature.[81] The resultant polymer from the template molecule recognizes all the binding sites from the template molecules. There are two types of molecular imprinting techniques, which are the self-assembling and preorganized approach.[81,82] The self-assembling approach was reported, and it is very similar to the biological recognition systems.[82] This approach of interactions between the polymer template and polymer uses hydrogen bonds, dipole-dipole, Van der Waals forces, non-covalent forces, and functional groups present in the polymer matrix drive the molecular recognition phenomena.

1.4 Experimental

The following constitutes the rationale for developing an experimental procedure, found in this section.

1.4.1 Materials

The materials and sources are aluminum nitrate (Fisher Scientific Co., 99.2%), magnesium nitrate (Fisher Scientific Co., 99.9%), sodium hydroxide (Fisher Scientific Co., 99.6%), benzoic acid (Fisher Scientific Co.,), sodium persulfate (Aldrich Chemical Company, Inc., 98%), sodium dodecyl sulfate (SDS) (Sigma Chemical Co., 99%),

potassium dichromate (Fisher Scientific Co., 99.6%), sulfuric acid (Fisher Scientific Co., 98%), propan-1-ol (Across Organic Co., 99.5%), toluene, trans,-trans-1,3 butadiene-1,4-dicarboxylic acid, sodium persulfate, and allyl alcohol were all used as received.

1.4.2 Preparation of $Mg_3Al(OH)_8NO_3{\cdot}2H_2O$

$Mg_3Al(OH)_8NO_3{\cdot}2H_2O$ (Mg_3/Al-LDH-$NO_3{\cdot}2H_2O$) prepared by co-precipitation resulting from the addition of a mixed metal acid solution to a basic solution. $Mg(NO_3)_2{\cdot}6H_2O$ of 5 g dissolved in 69 mL of distilled water, and $Al(NO_3{\cdot}9H_2O$ of 5 g was dissolved in 23 mL of distilled water separately before being mixed for the preparation of the mixed metal acid solution. The mixed metal acid solution was transferred into a clean 150 mL separatory funnel. A solution containing 7.0 g of sodium hydroxide dissolved in 150 mL of distilled water transferred into a separatory funnel, and then 60 mL of distilled water placed into the three-neck flask and the separatory funnels were attached. The metal mixture was then slowly added dropwise into a three-neck round flask, and the pH maintained at 10 using the sodium hydroxide solution. The LDH synthesis completed when all of the mixed metal acids added to the three-neck round flask. This took about 20 to 25 minutes. The resulting slurry was placed in a hot water bath for 24 hours at 70°C for the formation of the crystals.

$$3Mg\,(NO_3)_2 + Al\,(NO_3)_3 + 8NaOH + 2H_2O \rightarrow Mg_3Al(OH)_8NO_3{\cdot}\ 2H_2O + 8NaNO_3$$

1.4.3 Preparation of $Mg_3Al(OH)_8C_{12}H_{25}SO_4 \cdot 2H_2O$

$Mg_3Al(OH)_8C_{12}H_{25}SO_4 \cdot 2H_2O$ (Mg_3/Al-LDH- $C_{12}H_{25}SO_4 \cdot 2H_2O$) prepared by anion exchange resulting from $Mg_3Al(OH)_8NO_3 \cdot 2H_2O$ and sodium dodecyl sulfate (SDS) solution. Sodium dodecyl sulfate of 3 g was dissolved in 100 mL of distilled water and transferred into a round flask. $Mg_3Al(OH)_8NO_3 \cdot 2H_2O$ of 5 mL mixed with 10 mL of sodium dodecyl sulfate solution carried out under nitrogen while stirring. The pH value of the mixed solutions was kept at 9 using sodium hydroxide solution. The mixture was kept at room temperature for 24 hours while stirring. The precipitate from the LDHs was washed with distilled water and dried under nitrogen at 70°C.

$$Mg_3Al(OH)_8NO_3 \cdot 2H_2O + C_{12}H_{25}SO_4 \rightarrow Mg_3Al(OH)_8C_{12}H_{25}SO_4 \cdot 2H_2O + NaSO_4$$

1.4.4 Preparation of $Mg_3Al(OH)_8(S_2O_8)_{1/2}$

$Mg_3Al(OH)_8(S_2O_8)_{1/2}$ (Mg_3/Al-LDH- $S_2O_8 \cdot 2H_2O$) prepared by anion exchange resulting from $Mg_3Al(OH)_8NO_3 \cdot 2H_2O$ and sodium persulfate ($Na_2S_2O_8$) solution. Sodium persulfate of 12 g was dissolved in 100 mL of distilled water and transferred into a round flask. $Mg_3Al(OH)_8NO_3 \cdot 2H_2O$ of 10 mL mixed with 10 mL of sodium persulfate solution carried out under nitrogen while stirring. The pH value of the mixed solutions kept at 9. The mixture was kept at room temperature for 24 hours while stirring. The precipitate from the LDHs was washed with distilled water and dried under nitrogen at 70°C.

1.4.5 Preparation of $Mg_3Al(OH)_8(C_{12}H_{25}SO_4)_{1-x}(S_2O_8)_{x/2}$

$Mg_3Al(OH)_8(C_{12}H_{25}SO_4)_{1-x}(S_2O_8)_{x/2}$ (Mg_3/Al-LDH- $C_{12}H_{25}SO_4$/ $S_2O_8{\cdot}2H_2O$) prepared from $Mg_3Al(OH)_8NO_3{\cdot}2H_2O$, sodium persulfate ($Na_2S_2O_8$) and sodium dodecyl sulfate solution. $Mg_3Al(OH)_8NO_3{\cdot}\ 2H_2O$ of 5 mL, 5 mL of sodium persulfate, and 10 mL of sodium dodecyl sulfate solutions were all mixed and carried out under nitrogen while stirring. The pH value of the mixed solutions was kept at 9 using sodium hydroxide solution. The mixture was kept at room temperature for 24 hours while stirring. The precipitate from the LDHs was washed with distilled water and dried under nitrogen at 70°C.

1.4.6 Potassium Dichromate Reagent

The oxidizing agent used in the alcohol investigation contained potassium dichromate (VI) acidified with dilute sulfuric acid. If the oxidation is complete, the dichromate (VI) ions turn green solution containing chromium (III) ions shown in the electron half equation below.[83] Potassium dichromate with sulfuric acid mixed with ethanol and $Mg_3Al(OH)_8C_{12}H_{25}SO_4{\cdot}2H_2O$.

$$Cr_2O_7^{2-} + 14H^+ + 6e^- \rightarrow 2Cr^{3+} + 7H_2O$$

In a 10 mL volumetric flask, 5 mL of $Mg_3Al(OH)_8C_{12}H_{25}SO_4{\cdot}2H_2O$, 1 mL of dichromate, 1 mL of sulfuric acid, and 3 mL of ethanol were mixed and stirred. The mixture placed into an oil bath at 30°C. A small portion of the solution was transferred from the volumetric flask into a cuvette and analyzed using UV/Vis spectrophotometer.

1.4.7 Amount of Alcohol Absorbed by LDHs

$Mg_3\ Al(OH)_8C_{12}H_{25}SO_4{\cdot}\ 2H_2O \cdot CH_2{=}CHCH_2OH$ prepared from $Mg_3\ Al(OH)_8C_{12}H_{25}SO_4{\cdot}\ 2H_2O$ and allyl alcohol. $Mg_3Al(OH)_8C_{12}H_{25}SO_4{\cdot}\ 2H_2O$ of 3 mL was measured out and transferred into six different 10 mL volumetric flasks. Each of the five volumetric flasks contained additional (1mL, 2mL, 4mL, and 6mL, respectively) of allyl alcohol. Distilled water used to complete the total volume of the 10mL volumetric flasks. The solution was centrifuged at 2600 rpm for 15 minutes to separate both layers. The supernatant layer containing 8mL of $Mg_3\ Al(OH)_8C_{12}H_{25}SO_4{\cdot}\ 2H_2O \cdot CH_2{=}CHCH_2OH$ transferred into another six 10 mL of volumetric flasks. An additional 1 mL of dichromate and 1 mL of sulfuric acid mixed and analyzed to determine the amount of alcohol absorbed in $Mg_3\ Al(OH)_8C_{12}H_{25}SO_4{\cdot}\ 2H_2O \cdot CH_2{=}CHCH_2OH$. The mixture placed into an oil bath at 30°C. A small portion of the solution was transferred from the volumetric flask into a cuvette and analyzed using UV/Vis spectrophotometer.

1.4.8 Characterization

Powder x-ray diffraction data were recorded on a PANalytical diffractometer using CuKα radiation (1.54187 Å) at 45 kV and 40mA. The crystalline sample placed in

the center of the instrument before being hit by the x-ray at angles of 2° to 70°. The basal-spacing calculated using the diffraction maxima. Powder x-ray diffraction samples containing LDHs ground in a mortal with a pistol. The ground samples were then placed in the middle of the powder x-ray diffraction plate and placed into the instrument.

Fourier transform infrared spectroscopy (4000 – 400 cm^{-1}) using a Nicolet 1700 FT-IR spectrometer was used to identify the functional groups. Fourier transform infrared spectroscopy samples placed in a mortal and ground with a pestle. LDH samples ground with potassium bromide. Fourier transform infrared spectroscopy was calibrated using potassium bromide before the mixture of LDHs and potassium bromide was placed into the sample holder. The sample holder containing the sample placed into the instrument.

Thermogravimetric analysis of samples was carried out in the air between 0 to 600°C. The morphology of the Mg^{2+}/Al^{3+}-LDH samples was studied using a scanning electron microscope. Optical absorbance determined by a UV-Vis spectrophotometer (Cary 100 Bio).

1.4.9 LDHs Sample Preparation

The sample preparation varies for each characterization used to analyzed LDHs. Powder x-ray diffraction sample containing LDHs grounded inside a mortal with a pistol. The grounded sample was then placed in the middle of the powder x-ray diffraction plate and placed into the instrument. Fourier transform infrared spectroscopy (FTIR) prepared

inside a mortal with a pistol. LDHs sample grounded with potassium bromide (KBr). Fourier transform infrared spectroscopy was calibrated using potassium bromide before the mixture of LDHs and potassium bromide was placed into the sample holder. The sample holder containing the sample placed into the instrument. The preparation to absorbed alcohol using a UV-Vis spectrophotometer (Cary 100 Bio) carried out in 10 mL of volumetric flask. Each flask contained different volumes of Mg_3 $Al(OH)_8C_{12}H_{25}SO_4 \cdot 2H_2O \cdot CH_2{=}CHCH_2OH$ with dichromate and sulfuric acid.

1.5 Results and Discussion

It is proposed that the galleries of layered double hydroxides can serve as controlled environments in which to carry out polymerizations of organic monomers. Such a controlled environment would potentially be able to control the morphology of the resulting polymer, the distribution of monomers in copolymers, the accessibility of the imprints in imprinted polymers, and several other properties. The radical polymerization of anionic monomers in the galleries of layered double hydroxides has successfully carried out. Of interest in this investigation is the polymerization of neutral monomers in the galleries of layered double hydroxides with the ultimate long-term goal of synthesizing imprinted polymers that can bind specific drugs in an effort to eliminate the problems caused by the distribution of counterfeit drugs.

Layered double hydroxides consist of positively charged metal-hydroxide layers that are separated by galleries that can absorb anions ranging from atomic anions to huge

molecules such as DNA.[69] Because these galleries are lined with a hydroxyl group, the gallery environment is necessarily homophilic. The monomers of interest, being nonpolar organic molecules, however, are hydrophilic. This being the case, the interiors of the galleries have to be made hydrophobic in order for the monomers of interest to be absorbed into the galleries. Towards this end, it proposed that the interior of the galleries be made hydrophobic by replacing the inorganic anions in the galleries with anions having large hydrophobic segments. In addition, in order to properly initiate the polymerizations in the galleries, the initiators must also be in the galleries. In order to accomplish this, it proposed that anionic initiator ions be co-absorbed onto the walls of the galleries.

1.5.1 Layered Double Hydroxide: Starting Materials

The layered double hydroxide, containing magnesium and aluminum as metals, is the most thoroughly investigated layered double hydroxide. The aluminum-magnesium layered double hydroxide having magnesium to aluminum ratio of three and nitrate as the anion in the galleries was selected as the starting material, $AlMg_3(OH)_8NO_3 \cdot 2H_2O$. This was prepared by the treatment of a solution of the nitrate salts of aluminum and magnesium with a sodium hydroxide solution while maintaining the pH at or near 10.

$$Al(NO_3)_3(aq) + 3Mg(NO_3)_2(aq) + 8NaOH(aq) + 2H_2O \rightarrow$$

$$AlMg_3(OH)_8NO_3 \cdot 2H_2O\ (s) + 8NaNO_3(aq)$$

The resulting product was washed extensively and used as a slurry.

1.5.2 Mg/Al-LDH-NO_3 Infrared Analysis

The product was obtained as an aqueous slurry. Samples were dried under nitrogen for characterization purposes. The infrared spectra were obtained using the dried sample in a potassium bromide disc. The infrared (IR) spectrum and data (Figure 7 and Table 1) were obtained to identify each of the functional groups shown in Figure 7. The IR spectrum of this compound has a sharp, intense peak at 1384cm^{-1}, which has been assigned to intercalated nitrate ions. The broad, intense peak at 3465cm^{-1} indicates the presence of the hydroxide layer and interlayer water molecules. The absence of a peak or shoulder at 1368cm^{-1} indicates the absence of any carbonate in the galleries. Carbonate ions are a common contaminant, which might have formed during the synthesis. The broadband of the bending vibration of the interlayer H_2O is at 1638cm^{-1}, as expected. The band characteristic of metal-oxygen bond stretching appears below 825cm^{-1}. The broadband around 569cm^{-1} is caused by various lattice vibrations associated with metal-hydroxide sheets. Thus, the infrared analysis confirms the presence of the hydroxyl, nitrate, and intercalated water functionalities.

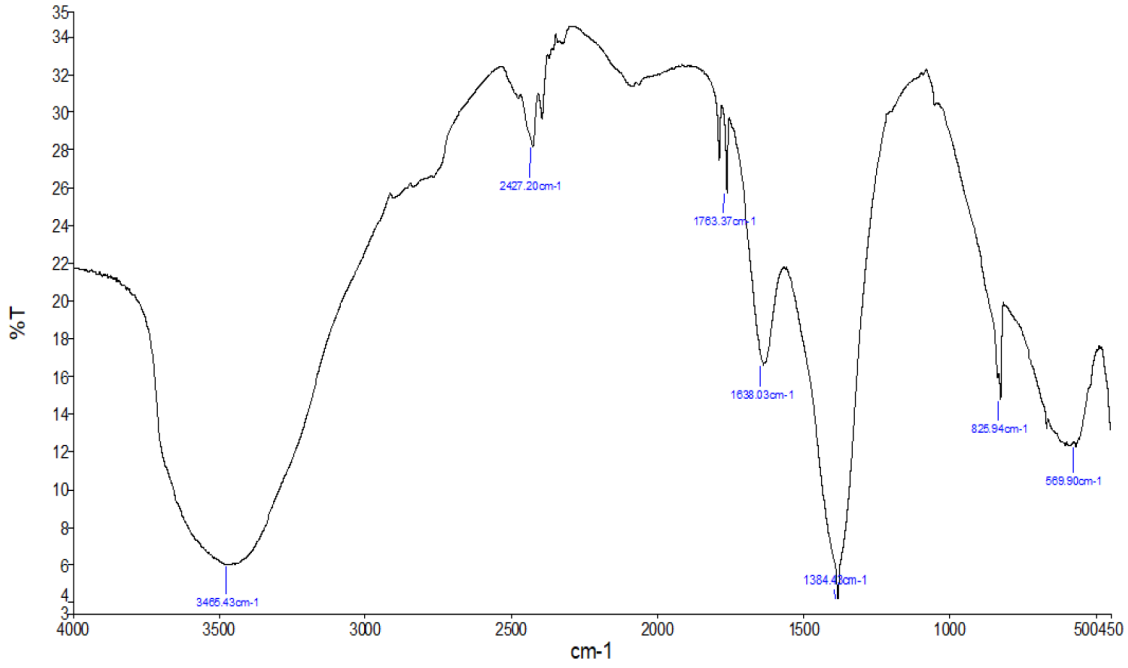

Figure 7. FTIR spectrum of Mg/Al-LDH-NO_3.

Table 1. Identification and Assignment of IR Bands of Mg^{2+}/Al^{3+}-LDH-$NO_3 \cdot 2H_2O$

Assignments	**Band Position/Range (cm^{-1})**	
	Literature[1]	**Observed**
O-H (Al/Mg-LDH)	3200-3700[a]	3000-3750
H-O-H	1637	1638
C-O (Al/Mg-LDH-CO_3)	1368[a]	absent
N-O ($NaNO_3$)	1386[b]	1384
O-M-O	492-600	500-750

1.5.3 Mg/Al-LDH-NO_3 X-Ray Diffraction Analysis

Whereas the infrared data (Table 2 and Table 3) showed the presence of OH^-, NO_3, and H_2O, the powder XRD results provide information about the solid-state structure of the LDH (Figure 9 and Figure 10), in particular the basal spacing, the and crystallinity of the crystals as well as the presence of other possible crystalline phases. The basal spacing is the distance from the center of one metal-hydroxide layer and the next. It serves as a measure of the height and volume of the galleries of the LDH. This spacing is very sensitive to the characteristics of the interlayer anions.

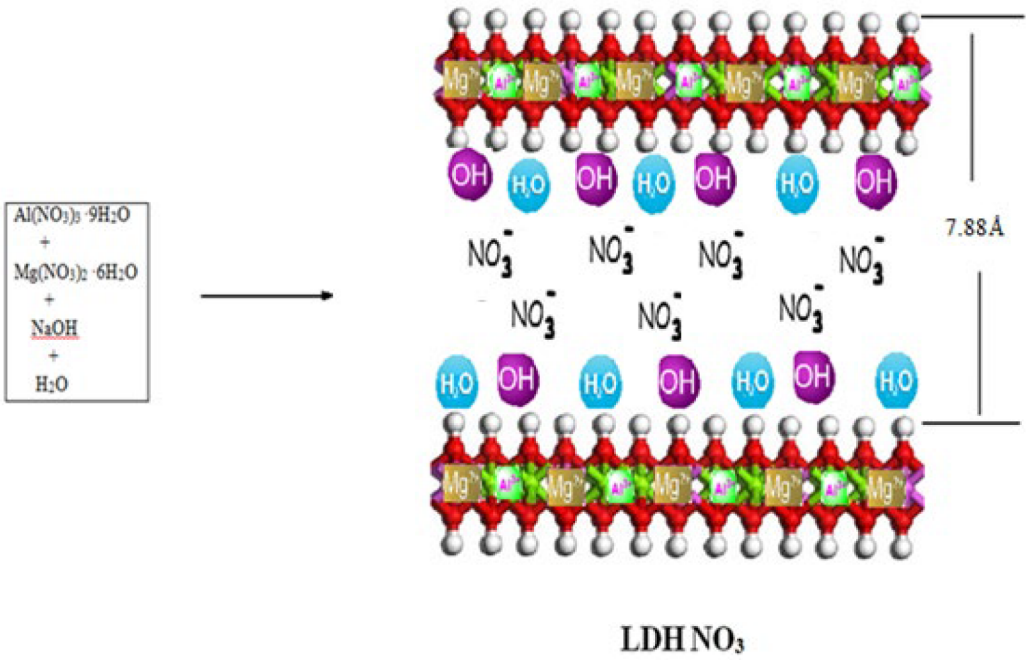

Figure 8. Schematic diagram of Mg/Al-LDH-NO_3.

X-ray diffractograms data obtained for Al/Mg-LD-NO_3, prepared by both the coprecipitation and the ion exchange methods (Figures 9 and Figure 10). The data found in Tables 2 and Table 3. Presence in both cases of strong first, second, and third-order peaks that arise from a layered structure are strong indicators of presence metal-hydroxide layers with galleries in between. Furthermore, the relatively narrow full-widths-at-half-maxima (1.1 and 1.3 for the first order peaks obtained from samples prepared by the ion exchange and coprecipitation methods, respectively) show a high degree order among the sheets. The computed basal spacings are 7.85 and 7.95 Å for samples prepared by the ion exchange and coprecipitation methods, respectively. These interlayer spacings are very similar to those obtained for 3:1 (Mg to Al) Al/Mg-LDH-NO_3 reported in the literature.[68] The x-ray diffractograms of the Al/Mg-LDH-NO_3 in various literature reports show basal spacings of 7.90Å after drying in an oven for two days at 70°C.[4] These spacings suggest that the nitrate ion is in a tilted orientation in the interlayer region with its plane almost perpendicular to the hydroxide sheets.[4] The high crystallinity of Al/Mg -LDH-NO_3 is very important for the synthesis of Al/Mg-LDHs, for which Al/Mg -LD-NO_3 is a precursor. Drying under nitrogen has been reported to be the most effective way to avoid getting CO_3^{2-} into the galleries before carrying out subsequent anionic exchange reactions inside the galleries.

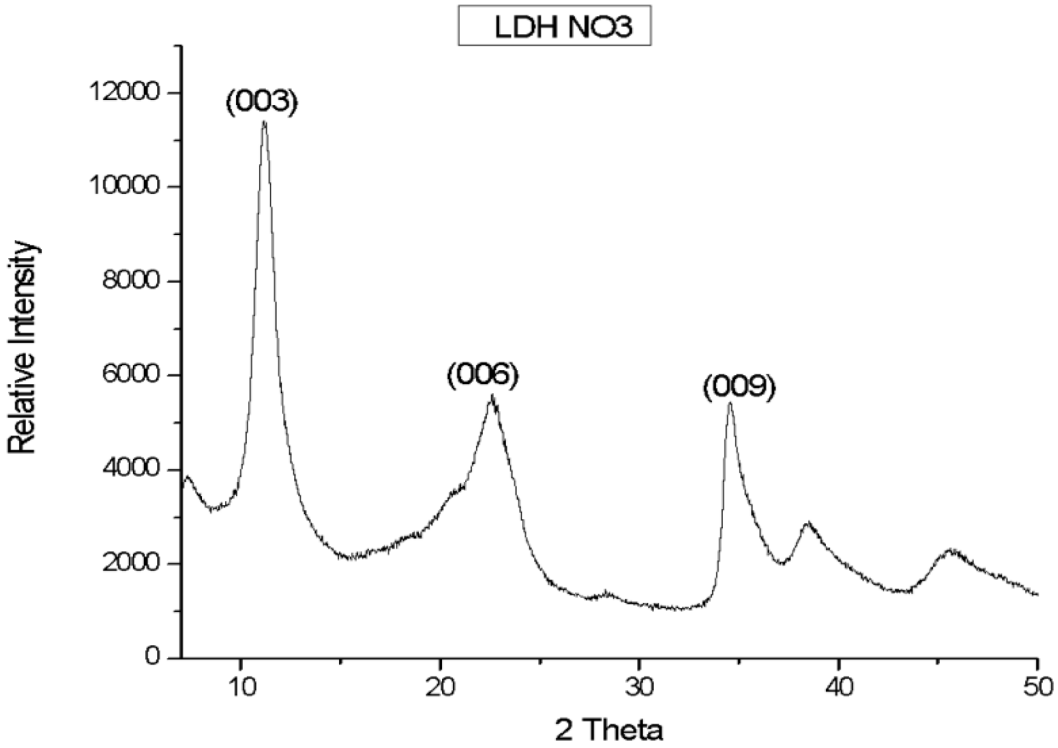

Figure 9. X-ray diffraction of Mg/Al-LDH NO_3 via the ion exchange method.

Table 2. Mg^{2+}/Al^{3+}-LDH NO_3 Basal Spacing Result via the Ion-exchange Method.

No.	Basal Spacing (Å)	2θ (°)	Intensity
1	7.90	11.2	9323.1
2	7.83	22.7	3727.5
3	7.84	34.3	2615.3

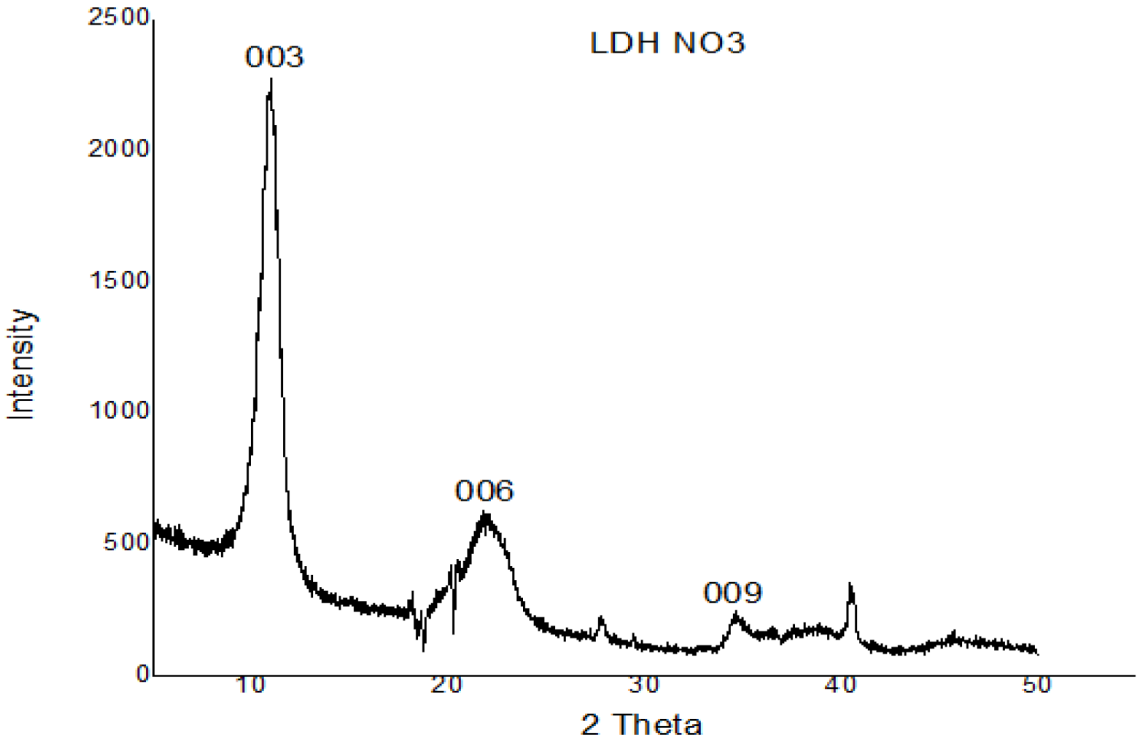

Figure 10. X-ray Diffraction of Mg/Al-LDH NO_3 via co-precipitation method.

Table 3. Mg/Al-LDH NO_3 Basal Result via the Co-precipitation Method.

No.	Basal Spacing (Å)	2θ (°)	Intensity
1	8.1	10.9	2271.6
2	8.1	21.9	613.08
3	7.7	34.8	215.59

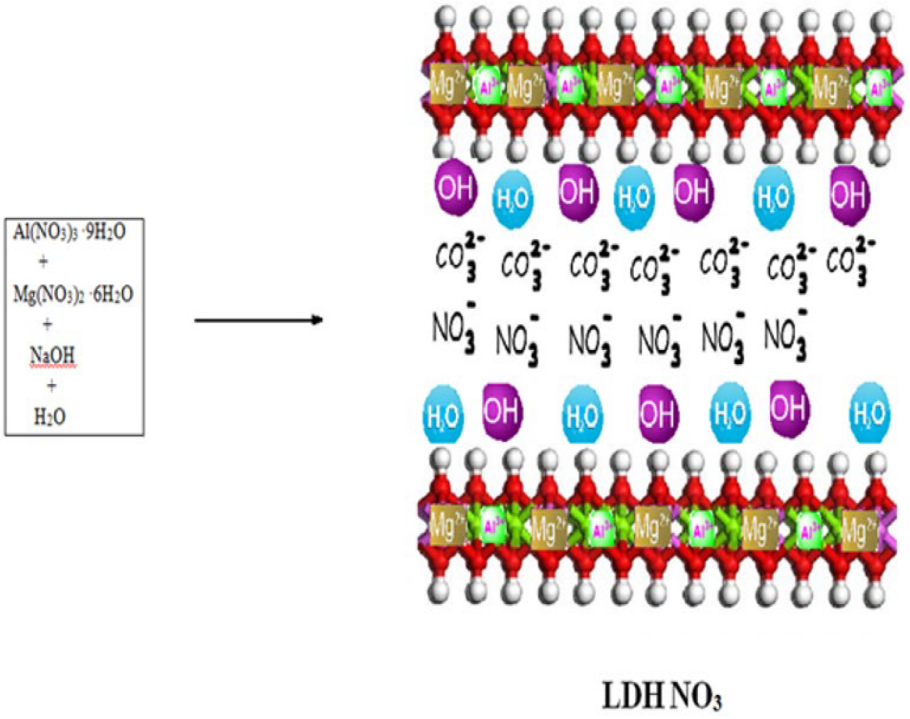

Figure 11. Schematic diagram of Mg/Al-LDH -NO_3 with carbonate ion.

1.5.4 Layered Double Hydroxides with Hydrophobic Galleries

It is proposed that to prepare a layered double hydroxide with hydrophobic galleries, the interior of the $AlMg_3(OH)_8NO_3{\cdot}2H_2O$ galleries will be resurfaced with long-chain hydrocarbons. The anions in the galleries of LDHs kinetically labile and can be replaced by other anions by an ion exchange process. It is proposed that resurfacing the galleries of $AlMg_3(OH)_8NO_3{\cdot}2H_2O$ with the dodecyl sulfate, which has a twelve-carbon chain bonded to a sulfate group, should yield hydrophobic galleries. $AlMg_3(OH)_8NO_3{\cdot}2H_2O$ was treated in aqueous solution under nitrogen with sodium

dodecyl sulfate (NaDS) to yield $AlMg_3(OH)_8(CH_3(CH_2)_{11}SO_4)\cdot nH_2O$ (Mg/Al-LDH-DS) (Figure 12), which obtained as an aqueous slurry.

$$CH_3(CH_2)_{11}SO_4Na + AlMg_3(OH)_8NO_3\cdot 2H_2O + (n\text{-}2)H_2O \rightarrow$$

$$AlMg_3(OH)_8(CH_3(CH_2)_{11}SO_4)\cdot nH_2O + NaNO_3$$

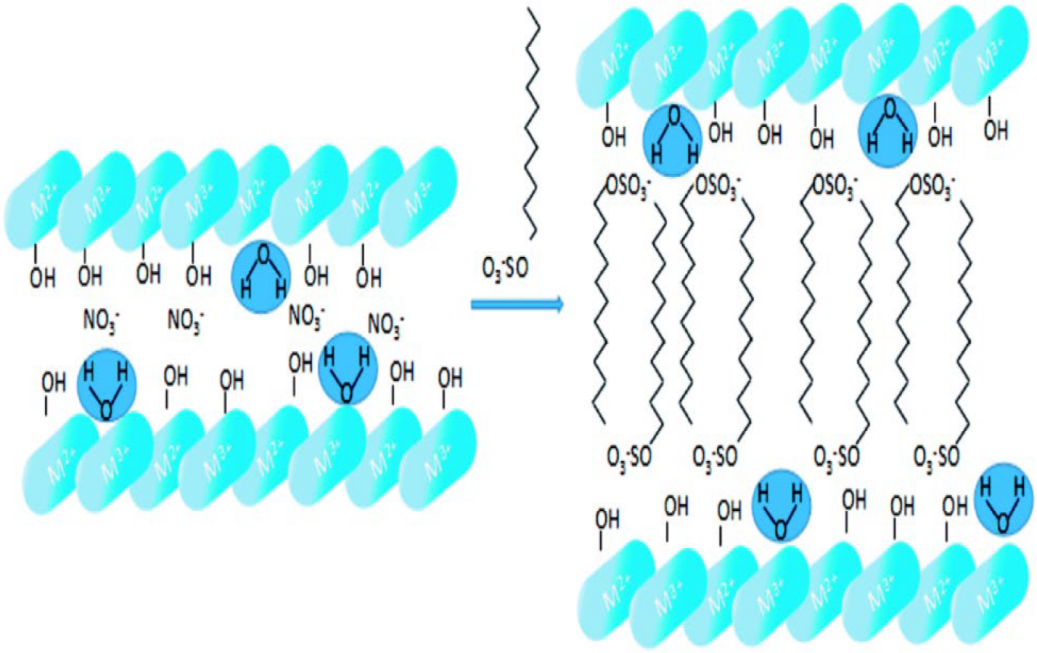

Figure 12. Schematic diagram of the synthesis of Al/Mg-LDH DS[70].

1.5.5 Mg/Al-LDH-DS Infrared Analysis

Samples were dried under nitrogen in a hot water bath for characterization purposes. Using a hot water bath at 70°C with a constant flow of nitrogen gas gives the same basal spacing as expected when the layered double hydroxide dried in an oven.[71] Figure 13 and Table 4 shows the IR spectrum of Al/Mg-LDH-DS. The broad absorption at 3500cm^{-1} is due to the O-H stretching vibrations of the hydroxyl groups and water molecules in the interlayer space. The peaks for the C-H stretching vibrations of the dodecyl sulfate in interlayer space observed at 2960, 2921cm$^{-1,}$ and 2849cm^{-1}. Peaks at 1210 cm^{-1}, 1080 cm$^{-1,}$ and 1019 cm^{-1} are assigned to S-O stretching vibration indicate the presence of the dodecyl sulfate. The absence of a peak at 1379cm^{-1} confirms the absence of nitrate ions in the Al/Mg-LDH-DS, which indicates the complete exchange of nitrate by the DS ion. Also, the absence of a peak at 1368 cm^{-1} confirms the absence of carbonate ions as a contaminant.

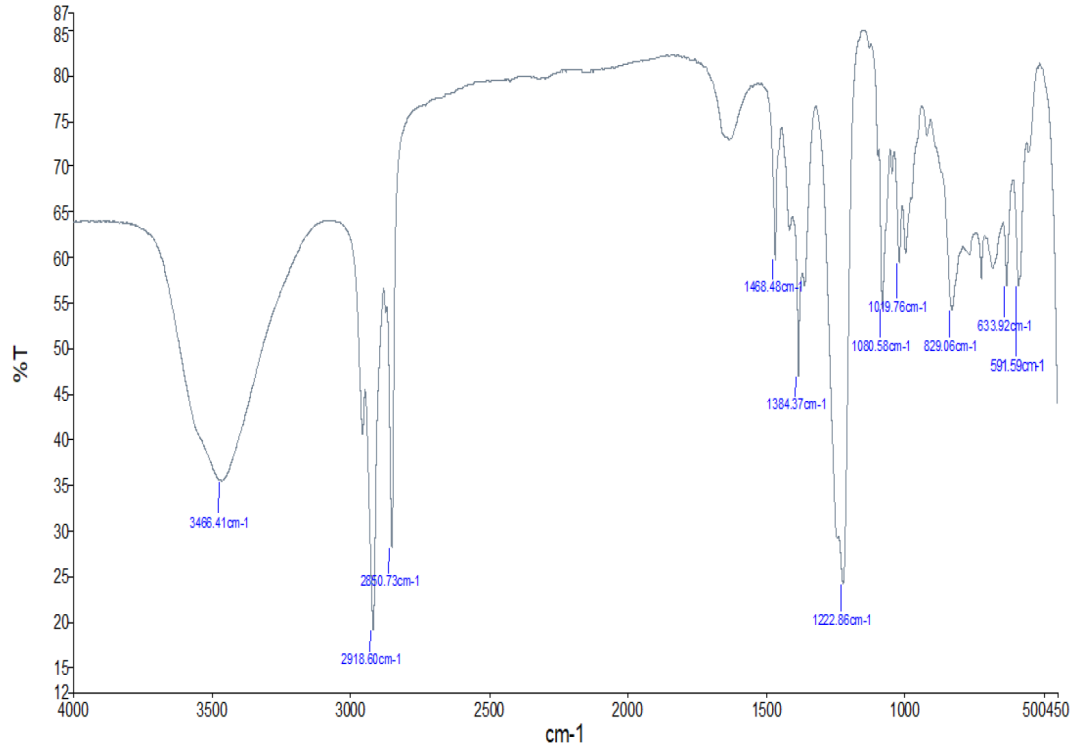

Figure 13. The infrared spectrum of Al/Mg-LDH-DS.

Table 4. Identification and Assignment of IR Bands of Al/Mg/Al-LDH-DS.

Assignments	**Band Position/Range (cm^{-1})**	
	Literature	**Observed**
O-H (Al/Mg-LDH)	3200-3700[a]	3000-3750
H-O-H	1637	1638
C-H	2900-2800	2960, 2921, 2849
C-O (Al/Mg-LDH-CO_3)	1368[a]	absent
S-O (Al/Mg-LDH-DS_3)	1210, 1062[c]	1210, 1080,1019
O-M-O	492-600	500-750

1.5.6 Mg/Al-LDH-DS X-ray Diffraction Analysis

The infrared results have shown that the interlayer nitrate ions have been completely replaced by dodecyl sulfate ions. Powder x-ray diffraction studies were carried out on a dried sample of Al/Mg-LDH-DS. The x-ray diffractogram may be found in Figure 14 and the data in Table 5. The first, second, and third-order peaks, which yield a basal spacing of 37.5Å, are clearly observed. The observed basal spacing is consistent with the basal spacing reported in the literature.[24] The large increase in basal spacing is consistent with the replacement of the comparatively small nitrate ion by one having a twelve-carbon chain.[71] The metal-hydroxide layer carries a net positive charge. Thus, the sulfate groups of the dodecyl sulfate ions are expected to line the surface of the metal-hydroxide layer, and the hydrocarbons tail extend into the interior of the galleries, making that portion of the galleries hydrophobic (Figure 14). The full-width-at-half-maximum for the first-order peak was only 0.4 Å, which is much smaller than that of Mg/Al-LDH-NO_3, from which it was prepared. This suggests that there was no loss in crystallinity during the conversion from nitrate to dodecyl sulfate. A number of factors impact the peak width. Among them are the crystallinity of the substance and the number of metal-hydroxide layers in the crystal. This being the case, the replacement of nitrate by dodecyl sulfate appears to have increased the crystallinity of the sample and/or to have increased the number of metal-hydroxide layers in the crystals.

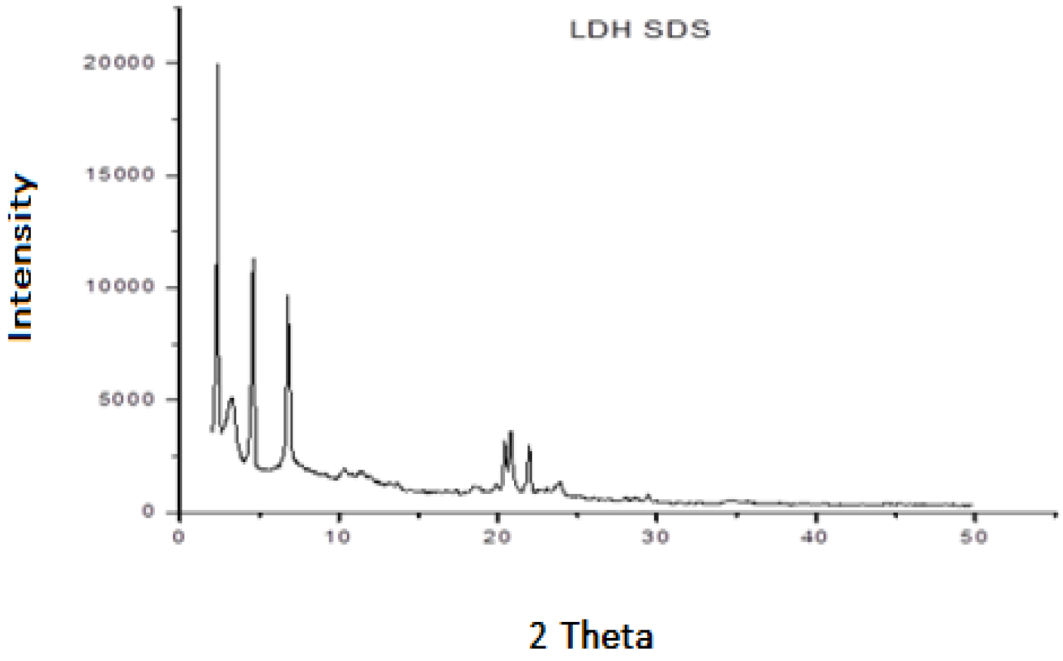

Figure 14. Powder x-ray diffractogram of Al/Mg-LDH-DS.

Table 5. X-ray Diffraction Data and Basal Spacings for Mg/Al-LDH-DS.

No.	**Basal Spacing (Å)**	**2θ (°)**	**Intensity**
1	35.9	2.46	19926
2	28.2	3.13	4940.8
3	37.9	4.66	11291
4	38.6	6.86	9127.2

1.5.7 Al/Mg-LDH-DS Thermogravimetric Analysis

Thermogravimetric analysis (TGA) is a thermal analysis method that measures the change in mass of a sample as its temperature is increased.[19] Thermalgravimetric analysis in the air was carried out on samples of Mg/Al-LDH-DS that had been dried under nitrogen (Figure 15). Since the drying procedure involved temperature no greater than seventy degrees, it is expected that only surface water would be removed. The interlayer water molecules are expected to reside near the surface of the metal-hydroxide layers, where hydrogen bonding and the charge of the sulfate of the dodecyl sulfate make the environment very hydrophilic. The thermograms show what appears to be three different decomposition processes, which are described in more detail in Table 6. For hydrotalcite, the quantitative loss of interlayer water occurs between 150 and 200 $^{\circ}C$ [d]

$$AlMg_3(OH)_8(C_{12}H_{25}SO_4)\cdot nH_2O \rightarrow AlMg_3(OH)_8(C_{12}H_{25}SO_4) + nH2O$$

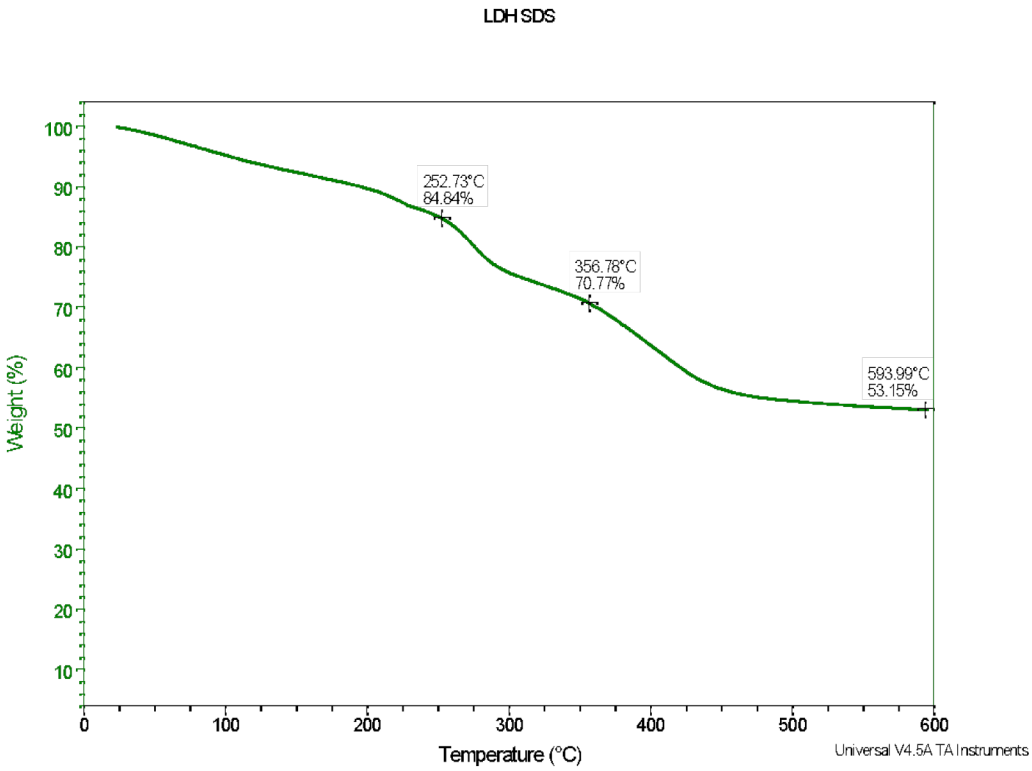

Figure 15. Thermogravimetric analysis of Mg/Al-LDH-DS in air.

Table 6. TGA Temperature Ranges

No.	Range	Change in Mass
1	25 °C → 245 °C	12 %
2	25 °C → 363 °C	30%
3	25 °C → 600 °C	44 %

The first loss in mass occurs below 245 °C. This being the case, the thermogram shows that the interlayer water accounts for 12 percent of the mass of the sample. Based on this result, the proper molecular formula for Mg/Al-LDH-DS should take the form

$AlMg_3(OH)_8(C_{12}H_{25}SO_4)\cdot 4H_2O$, in which the interlayer water is 12.6 % of the mass. It should be noted that the decrease in mass below 245 °C occurs in two stages, which suggests that the interlayer waters are not all equivalent.

Following the loss of the interlayer water (245 °C), there is an 18% decrease in mass. In hydrotalcite, this higher temperature process is attributed to dehydroxylation and decarbonylation. In the absence of carbonate ions, the loss of mass from 245 °C to 363 °C can be attributed to the decomposition of the layer hydroxides to yield metal oxides. This would account for 14.4% of the 18% decrease in mass.

$$AlMg_3(OH)_8(C_{12}H_{25}SO_4) \rightarrow AlMg_3O_4(C_{12}H_{25}SO_4) + 4H_2O$$

As the temperature is increased, there is an additional loss of mass, which is likely done to the decomposition of the dodecyl sulfate.

1.5.8 Mg/Al-LDH-DS Morphology

For the proposed applications, the morphology of the layered double hydroxides is very important. In order to be used as nano-reactors, a well-organized structure having uniform galleries is required for desired control over the reactions. However, layered double hydroxides have been reported that consist of hexagonal crystals on the micro-scale. Such structures are not optimal, because although they have uniform galleries,

would they wound inhibit diffusion of reactants into the galleries. With this in mind, the morphology of the Mg/Al-LDH-DS was characterized using scanning electron microscopy (SEM) shown in Figure 16, Figure 17, and Figure 18.

At lower magnification (14,378x), the Mg/Al-LDH-DS sample appears to be amorphous masses with voids, through which reactants can diffuse. Although at lower resolution (14,378x) Mg/Al-LDH-DS appears to be amorphous, at a higher resolution (66,887x), these amorphous masses appear to be composed of randomly oriented folded sheets separated by voids, which could fill with solvent, and allow access of reactants to the layer surfaces. The larger of these folded sheets are as much as 675 nm (6750 Å) across and 25 nm (250 Å) thick. It has already been determined that the basal spacing for Mg/Al-LDH-DS is 37.5 Å (Table 4), which means that these random foaled sheets contain approximately seven layers, and thus, contain about six galleries per sheet. The bulk material, having an open structure consisting of voids and sheets of only about seven layers, would be expected to be favorable for incorporating reactants into its galleries.

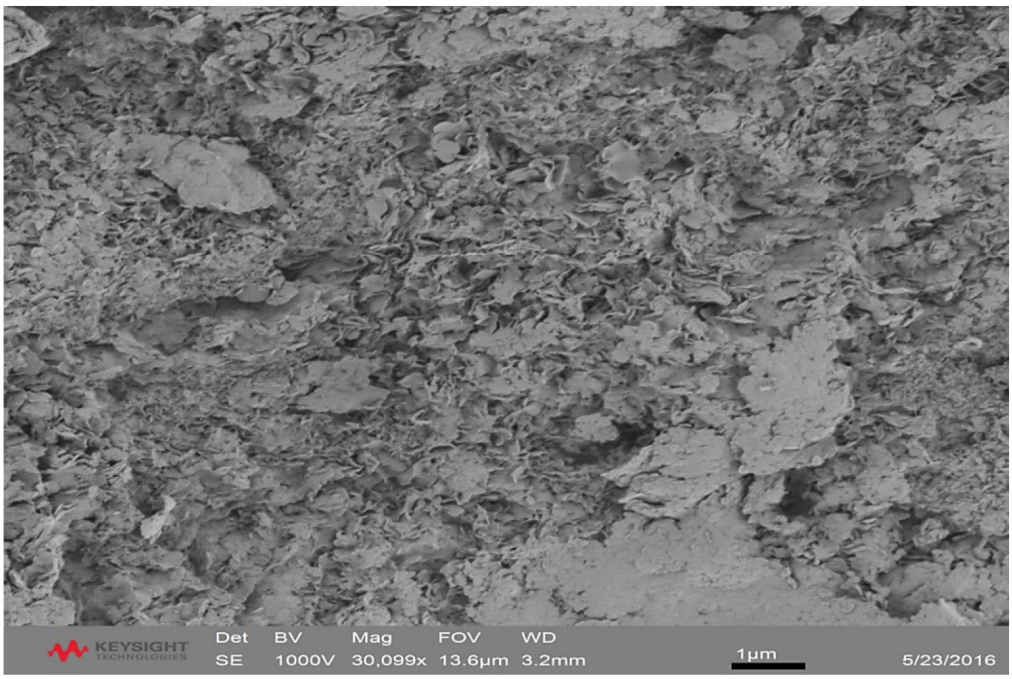

Figure 16. SEM of Mg/Al-LDH-DS at 30,099x.

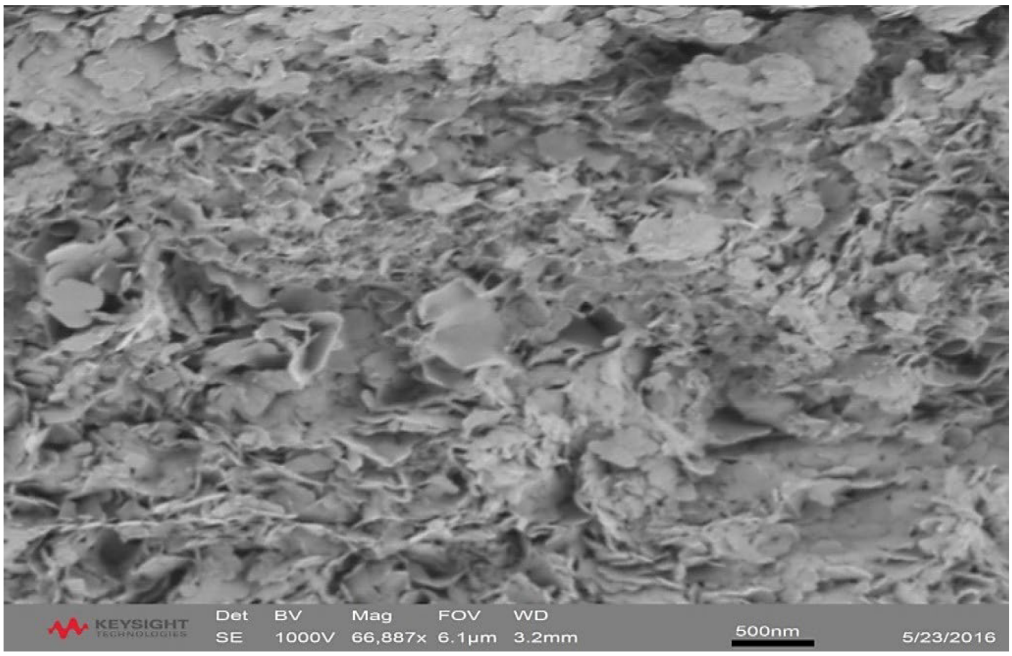

Figure 17. SEM of Mg/Al-LDH-DS at 66.887x.

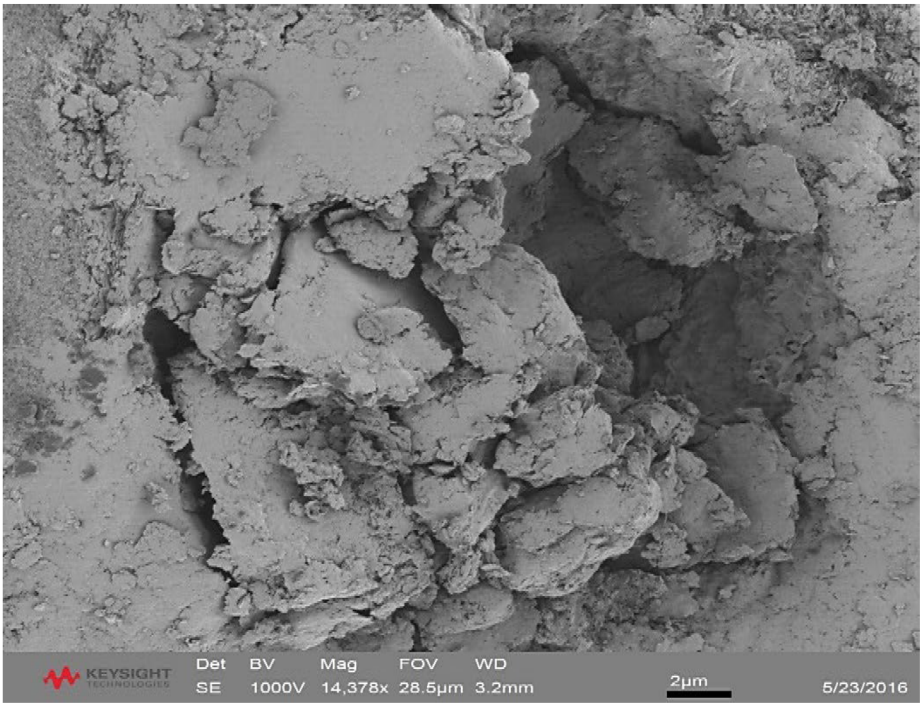

Figure 18. SEM of Mg/Al-LDH DS at 14,378x.

1.5.9 Layered Double Hydroxide with Free Radial Initiators

If layered double hydroxide galleries are to serve as nano-reactors for free-radical polymerizations, an initiator must be incorporated into the galleries at low concentrations. The persulfate ion is one of the most common ions used to generate free radicals when heated. [72]

$$S_2O_8^{2-} \rightarrow 2SO_4^{\cdot-}$$

$$SO_4^{\cdot-} + RHC{=}CH_2 \rightarrow \cdot CHR\text{-}CH_2SO_4^-$$

Although in order for the persulfate ion to be an effective initiator, it must be present in very low concentrations, at this stage, the objective was only to determine if

persulfate will intercalate into the galleries of the magnesium-aluminum layered double hydroxides. Being anionic, the persulfate ion can be incorporated into the galleries of Al/Mg-LDH-NO_3 via to the ion exchange reaction $2AlMg_3(OH)_8NO_3 + Na_2S_2O_8 \rightarrow 2AlMg_3(OH)_8(S_2O_8)_{1/2} + 2NaNO_3$ to yield $AlMg_3(OH)_8(S_2O_8)_{1/2}\cdot H_2O$ (Al/Mg-LDH-S_2O_8)

An aqueous slurry of $AlMg_3(OH)_8NO_3$ was treated with excess sodium persulfate at an elevated temperature. The product was obtained as a white slurry, which was thoroughly washed to remove excess persulfate. Samples were dried under nitrogen for characterization.

1.5.10 Mg/Al-LDH-S_2O_8 Infrared Analysis

The infrared spectrum of Al/Mg-LDH-S_2O_8 was recorded as a potassium bromide disk (Figure 19), and the results are tabulated in Table 7. As expected, the infrared spectrum contains the bands for the O-H stretching and bending vibrations at 3000-3750 cm^{-1} and 1631 cm^{-1}, respectively. The bands for the various metal-oxygen vibrations are found in the 500-700 cm^{-1} region. The assignment of the bands at 1159 cm^{-1} and 1116 cm^{-1} are similar in shape and separation to those found in $K_2S_2O_8$ but are shifted to higher energy. Unlike solid $K_2S_2O_8$, the persulfate ions in the galleries are likely to be hydrogen-bonded to the hydroxyl hydrogen atoms of the metal-hydroxide layer. This is likely to result in a shift in the vibrational bands. Additionally, the band for sulfate in K_2SO_4 is found at 1111 cm^{-1}. There is, however, a strong band at 1366 cm^{-1}, which is consistent

with the presence of carbonate ion. This suggests that there is carbonate contamination in this sample. The absence of a band at 1386 cm^{-1} shows that all of the nitrates in the starting material has been replaced. The three bands, 2432 cm^{-1}, 2388 $cm^{-1,}$ and 2092 $cm^{-1,}$ have not been assigned.

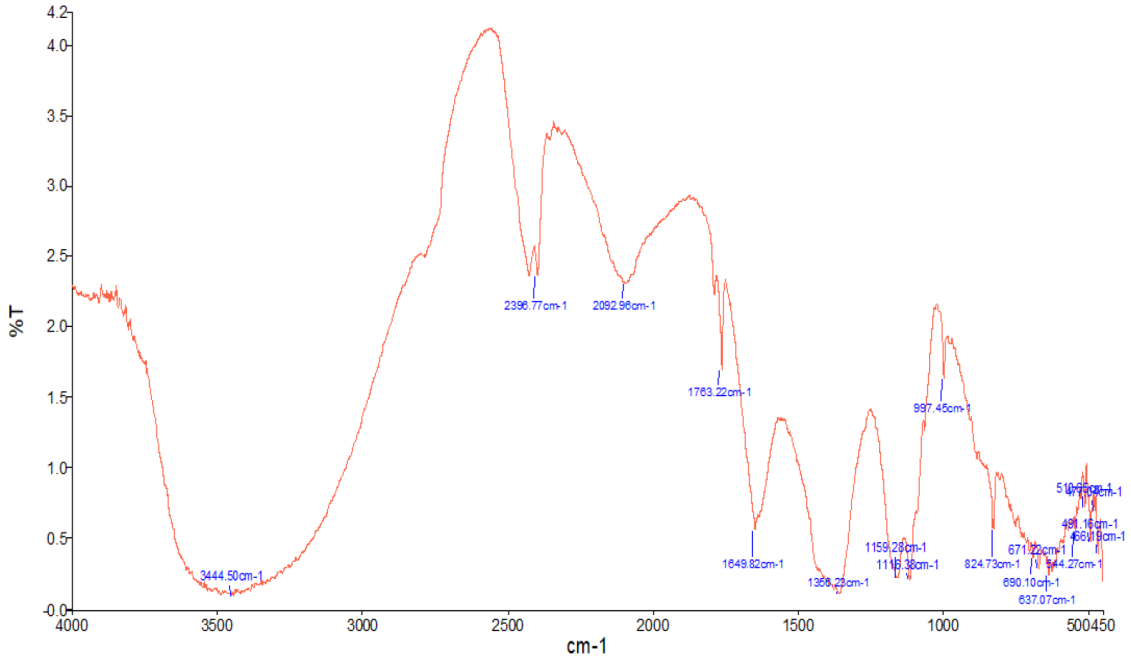

Figure 19. The infrared spectrum of Al/Mg-LDH-S_2O_8.

Table 7. Identification and Assignment of IR Bands of Al/Mg-LDH-S_2O_8.

Assignments	**Band Position/Range (cm^{-1})**	
	Literature	**Observed**
O-H (Al/Mg-LDH)	3200-3700[a]	3000-3750
H-O-H	1637	1631
H-C-C-H		2432
H-C-C-H		2388
H-C-C-H		2092
N-O ($NaNO_3$)	1386[b]	absent
C-O (Al/Mg-LDH-CO_3)	1368[a]	1366
S-O (Na_2SO_4)	1111[b]	1159,1115
S-O (K_2S2O_8)	1267,1304[b]	
O-M-O	492-600	500-750

1.5.11 Al/Mg-LDH-S_2O_8 X-ray Diffraction Analysis

Powder x-ray diffraction scans were carried out on a dried sample of Al/Mg-LDH-S_2O_8. The high noise to signal ratio and the increased baseline intensity at smaller angles suggest that this sample contains considerable amorphous material. This would be consistent with carbonate contamination. This notwithstanding, the first, second, and third-order reflections are apparent at 8.65°, 16.8°, and 24.7°. The powder x-ray diffractogram for Al/Mg-LDH-S_2O_8 is displayed in Figure 20, and the derivative data is tabulated in Table 8. The full-width-at-half-maximum is 1.8, which is greater than that for Al/Mg-LDH-NO_3, which was the starting material. This suggests that during ion exchange, there was a decrease in crystallinity and/or fewer layers per crystal. The first,

second, and third-order reflections are clearly apparent, and absent are peaks at 11.2°, 22.7°, and 34.3°, which indicates the absence of any significant Al/Mg-LDH-NO_3 phase.

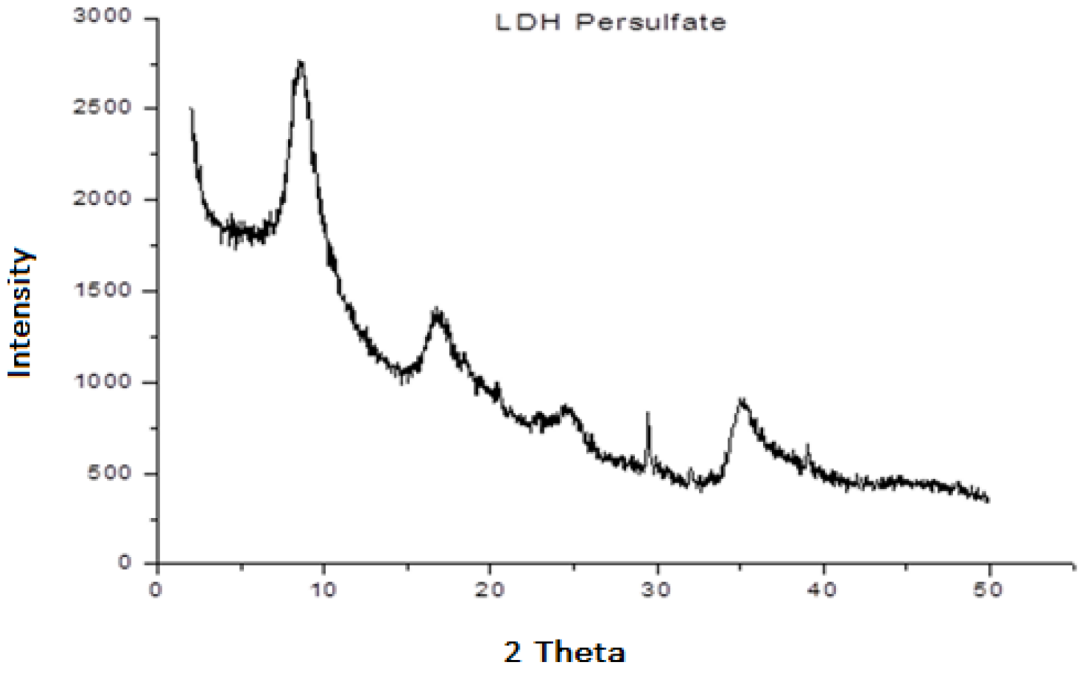

Figure 20. XRD of Al/Mg-LDH-S_2O_8.

Table 8. Mg/Al-LDH-S_2O_8.

No.	Basal Spacing (Å)	2θ (°)	Intensity
1	10.2	8.65	2739.1
2	10.5	16.8	1356.6
3	10.8	24.7	860.23

The observed basal-spacing is 10.5 Å, which is greater than that of Al/Mg-LDH-NO_3 (7.85 and 7.98 Å), from which Al/Mg-LDH-S_2O_8 was prepared and less than that of Al/Mg-LDH-DS, which has a much larger intercalated anion. Based on the structures of nitrate and persulfate ions (Figure 21), one would expect the long dimension of the persulfate to be more than twice that of the nitrate ion's longest dimension (Figure 21). However, the basal-spacing in Mg/Al-LDH-S_2O_8 is only 33 % greater than that in Al/Mg-LDH-NO_3, which suggests that the persulfate is oriented lengthwise on the surface of the metal-hydroxide layer. Such an orientation would allow for greater hydrogen bonding between the persulfate oxygens and the hydroxyl hydrogens as well as stronger electrostatic interactions.

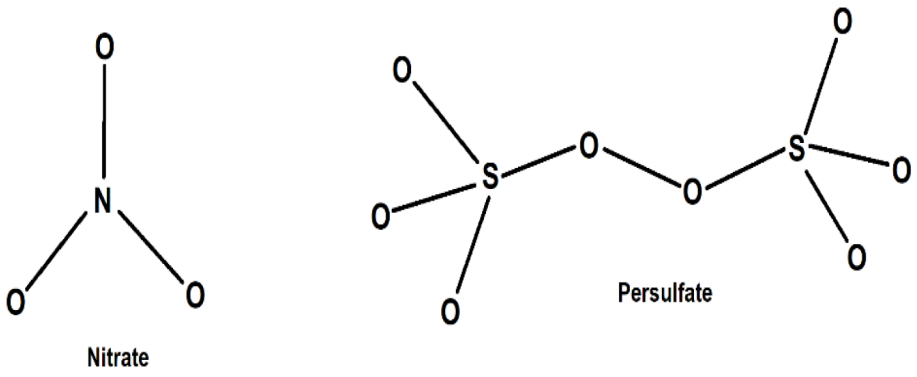

Figure 21. Schematic representations of the structures of nitrate and persulfate ions.

1.5.12 Hydrophobic Layered Double Hydroxides with Radical Initiators

There are two essential requirements for a layered double hydroxide nano-reactor to be used in the polymerization of olefins. These are a hydrophobic environment and the presence of a free radical initiator. In order to make the interior of the galleries hydrophobic, their surfaces have been lined with long-chain hydrocarbons. In order to incorporate a free radical initiator into the galleries, a layered double hydroxide has been prepared to contain the anionic persulfate ion. A functioning layered double hydroxide nanoreactor must contain both the anionic radical initiator and have an interior lined with long-chain hydrocarbons. Towards this end, a magnesium-aluminum layered double hydroxide was prepared that contained both intercalated dodecyl sulfate and persulfate.

1.5.13 Al/Mg-LDH-DS/S_2O_8 Infrared Analysis

The infrared spectrum of Al/Mg-LDH-S_2O_8 was recorded (Figure 22), and the results are tabulated in Table 9. As has been the case for the other LDHs, the infrared spectrum contains the bands for the O-H stretching and bending vibrations at 3000-3750 cm^{-1} and 1631 cm^{-1}, respectively. The bands for the various metal-oxygen vibrations are found in the 500-700 cm^{-1} region. The bands at 2957 cm^{-1}, 2919 $cm^{-1,}$ and 2851 cm^{-1} have been assigned to the C-H stretching vibrations of the dodecyl chain. The bands 1222 cm^{-1}, 1132 cm^{-1}, 1115 cm^{-1},1082 cm^{-1} and 1015 cm^{-1} are in the region of the S-O vibrations. Because both dodecyl sulfate and persulfate have S-O vibrations, it is difficult to assign these individual vibrations. These vibrations do compare favorably to

those of in the infrared spectra of Mg/Al-LDH- S_2O_8 and Mg/Al-LDH-DS recorded earlier (Figure 22 and Table 9). The absence of a band at 1368 cm^{-1} is a strong indication that this sample of free of carbonate contamination.

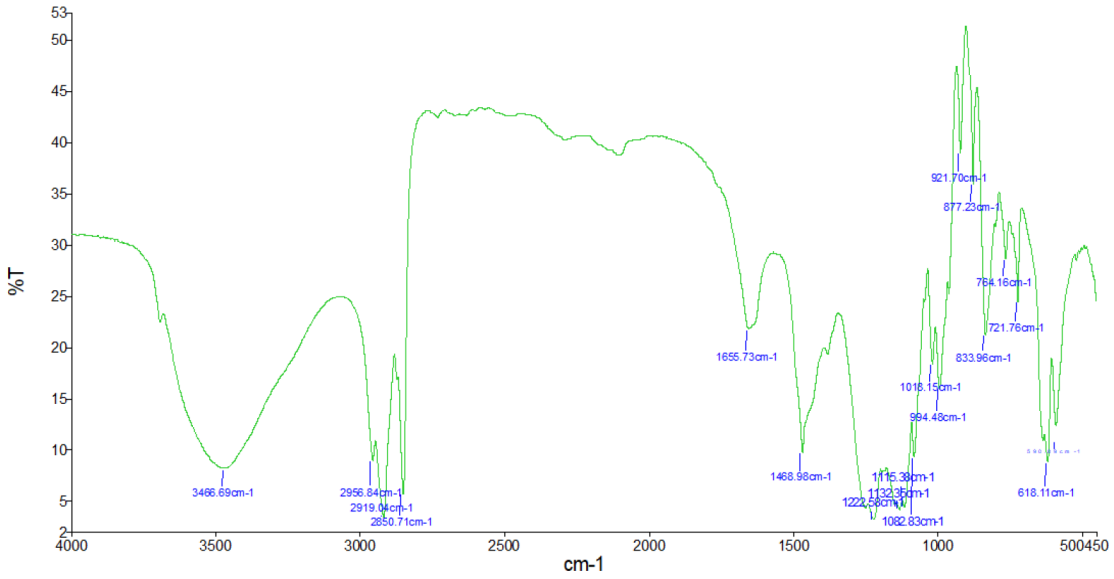

Figure 22. FTIR of Mg/Al-LDH-DS/S_2O_8.

Table 9. Identification and Assignment of IR Bands of Mg/Al-LDH-DS/S_2O_8.

Assignments	**Band Position/Range (cm^{-1})**	
	Literature	**Observed**
O-H (Al/Mg-LDH)	3200-3700[a]	3000-3750
H-O-H	1637	1659
C-H	2900-2800	2956, 2919, 2850
C-O (Al/Mg-LDH-CO_3)	1368[a]	absent
S-O (Al/Mg-LDH- S_2O_8)	1159,1115	1222, 1132, 1115, 1082, 1015
S-O (Al/Mg-LDH-DS)	1210, 1080, 1019	
O-M-O	492-600	500-750

1.5.14 Mg/Al-LDH-DS/S_2O_8 X-Ray Diffraction Analysis

Powder x-ray diffraction scans were carried out on a dried sample of Al/Mg-LDH-DS/S_2O_8. The very low noise to signal ratio suggests that this sample is very crystalline with little or no amorphous phase. The first, second, and third-order reflections are apparent at 2.44°, 4.92°, and 7.13°, shown in Figure 23 and Table 10. When attempting to intercalate two different anions into the same gallery of a layered hydroxide, one might form two or more different phases. One of the phases would contain exclusively one anion, the other phase would contain the other ion exclusively, and there might be another phase containing both ions. The x-ray diffraction results will determine if the co-intercalation of dodecyl sulfate and persulfate has been successful.

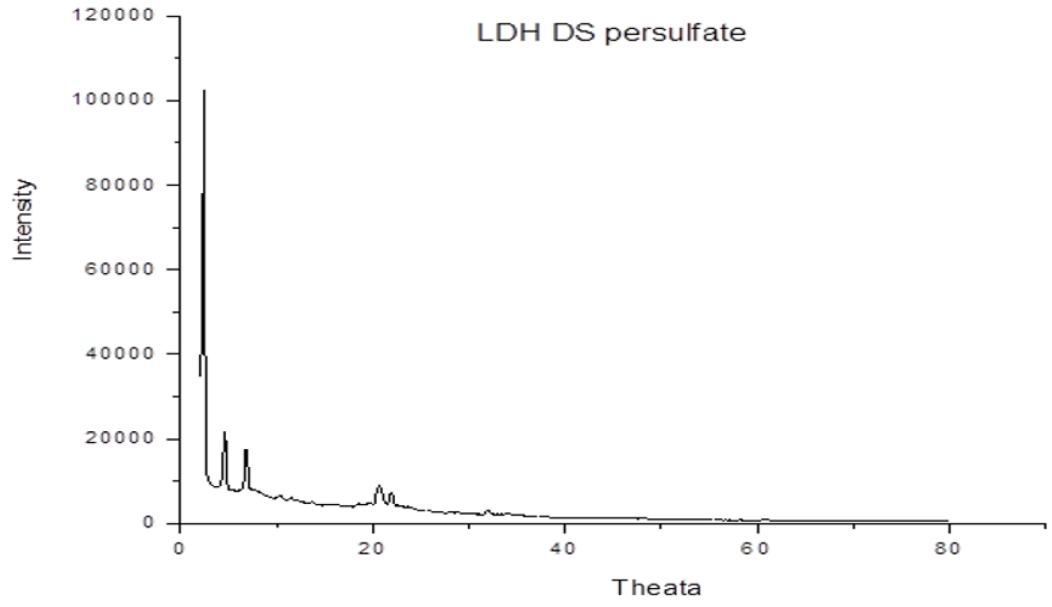

Figure 23. XRD of Mg/Al-LDH-DS/S_2O_8.

The first order reflections for Mg/Al-LDH-DS and Mg/Al-LDH-S_2O_8 are at 3.13° and 8.65°, respectively. The absence of these reflection shows that neither of these phases is present.

Table 10. LDH DS Persulfate Basal Spacing.

No.	Basal Spacing (Å)	2θ (°)	Intensity
1	36.2	2.44	102628
2	35.9	4.92	8802.51
3	37.2	7.13	8486.88

The basal spacing for Al/Mg-LDH-S_2O_8 is 10.5 Å, and that for Al/Mg-LDH-DS is 37.50.5 Å. The observed basal-spacing for Al/Mg-LDH-DS/S_2O_8 is 36.4 Å. It would, thus, appear that the persulfate in intercalated into the galleries along with dodecyl sulfate ions. As one might expect, the basal spacing for Al/Mg-LDH-DS/S_2O_8 is between that of Al/Mg-LDH-DS and Al/Mg-LDH-S_2O_8.

1.5.15 Mg/Al-LDH-DS/S_2O_8 Thermogravimetric Analysis

The presence of infrared bands for both dodecyl sulfate and for persulfate in the spectrum of Al/Mg-LDH-DS/S_2O_8 and a basal spacing between that of Al/Mg-LDH-DS and Al/Mg-LDH-S_2O_8 supports the co-intercalation of dodecyl sulfate and persulfate. The sample contained 14% intercalated water, which was lost between 25° to 244°. The

thermogravimetric scan is very similar to that of Mg/Al-LDH-DS. In the absence of a quantitative determination of the extent to which dodecyl sulfate was displaced by persulfate, it is difficult to provide a more detailed analysis shown in Figure 24 and Table 11.

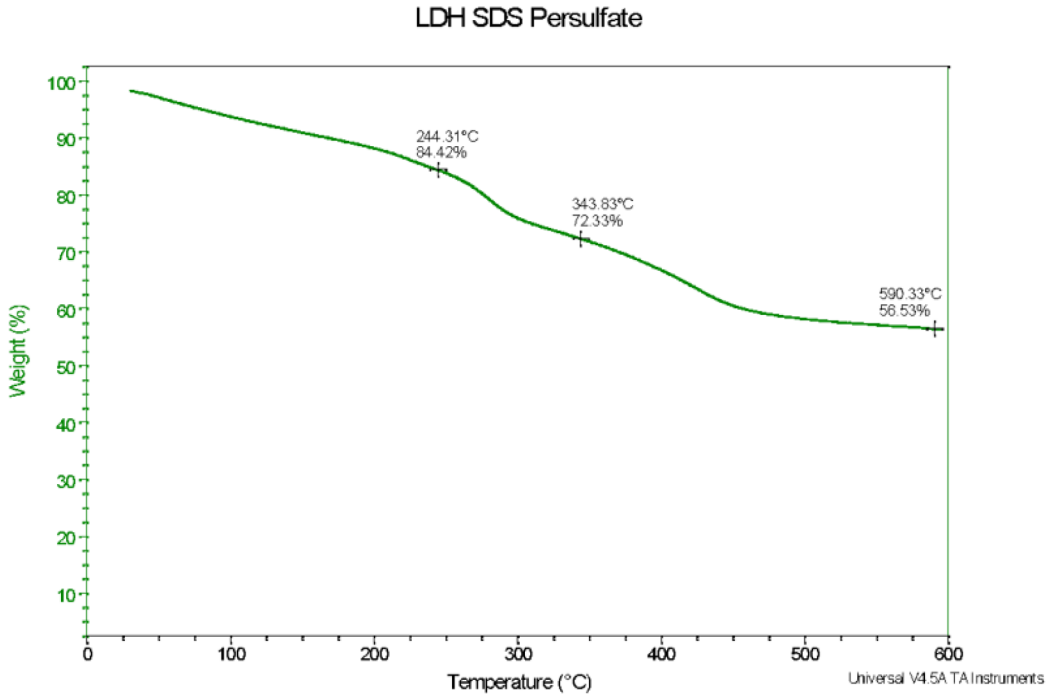

Figure 24. Thermogravimetric analysis of Al/Mg-LDH-DS/S_2O_8 in air.

Table 11. TGA Temperature Ranges

No.	Range	Change in Mass
1	25 °C → 244 °C	14 %
2	25 °C → 397 °C	33 %
3	25 °C → 600 °C	43 %

1.5.16 Mg/Al-LDH-DS/S_2O_8 Morphologies

The morphology of the Mg/Al-LDH-DS characterized using scanning electron microscopy (SEM). Although at lower resolution (14,378x), Mg/Al-LDH-DS/S_2O_8, like its precursor, appears to be amorphous at a higher resolution (75,051x), these amorphous masses appear to be composed of randomly oriented folded sheets separated by voids, which may fill with solvent. The folded sheets appear to have the same dimensions as those of the starting material (6750 Å across and 250 Å thick. It has been determined that the basal spacing for Mg/Al-LDH-DS/S_2O_8 is 37.5 Å (Table 10), which means that these sheets contain approximately seven layers, and thus, contain about six galleries per sheet.

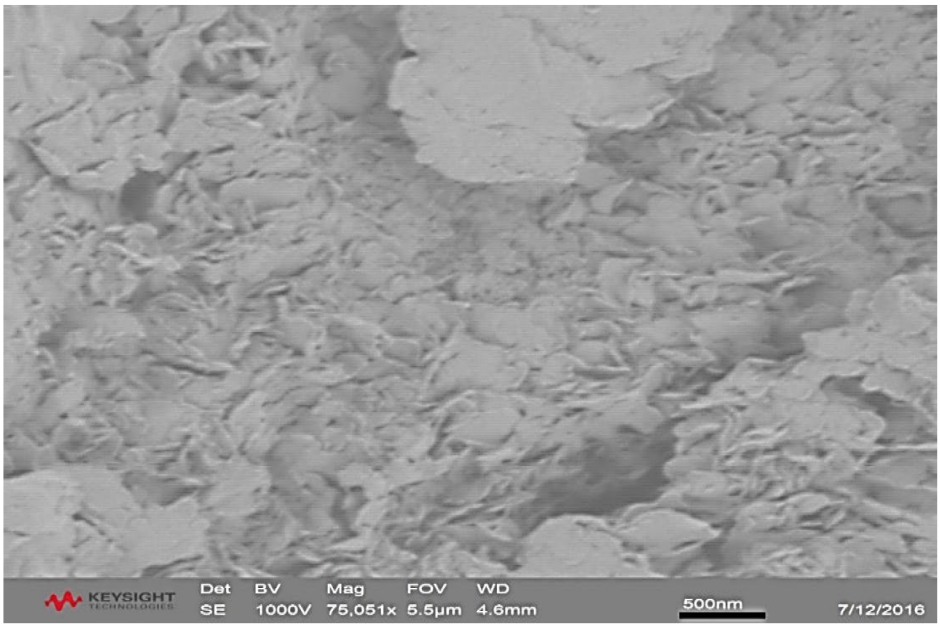

Figure 25. LDH DS Persulfate using SEM at 75,061x.

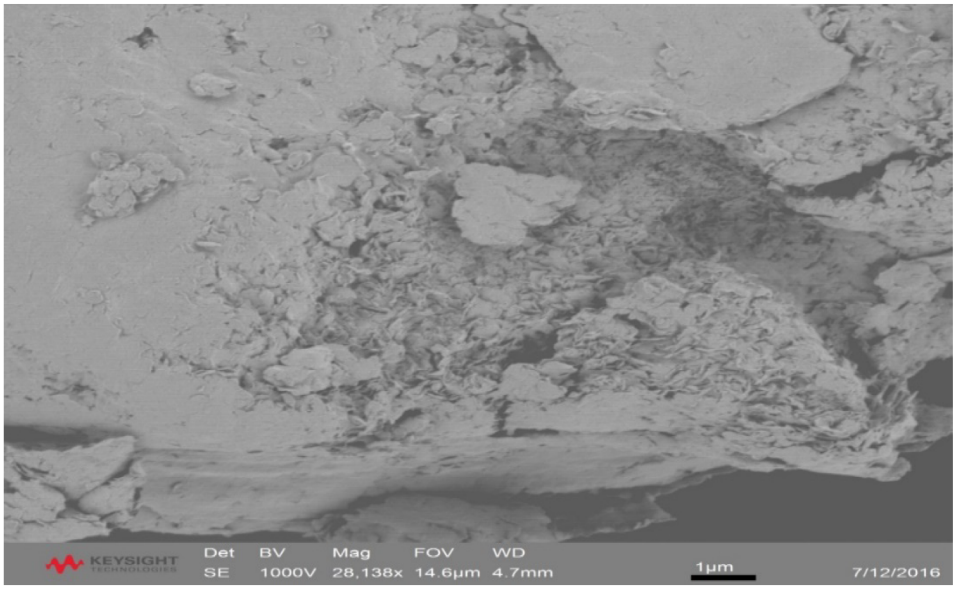

Figure 26. LDH DS Persulfate using SEM at 28,138x.

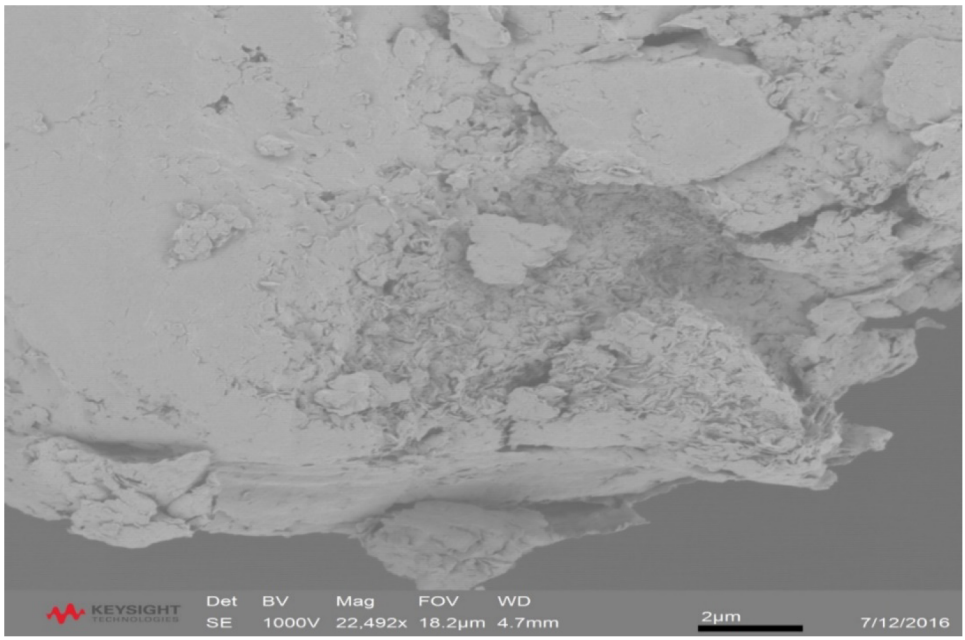

Figure 27a. LDH DS Persulfate using SEM at 22,492x

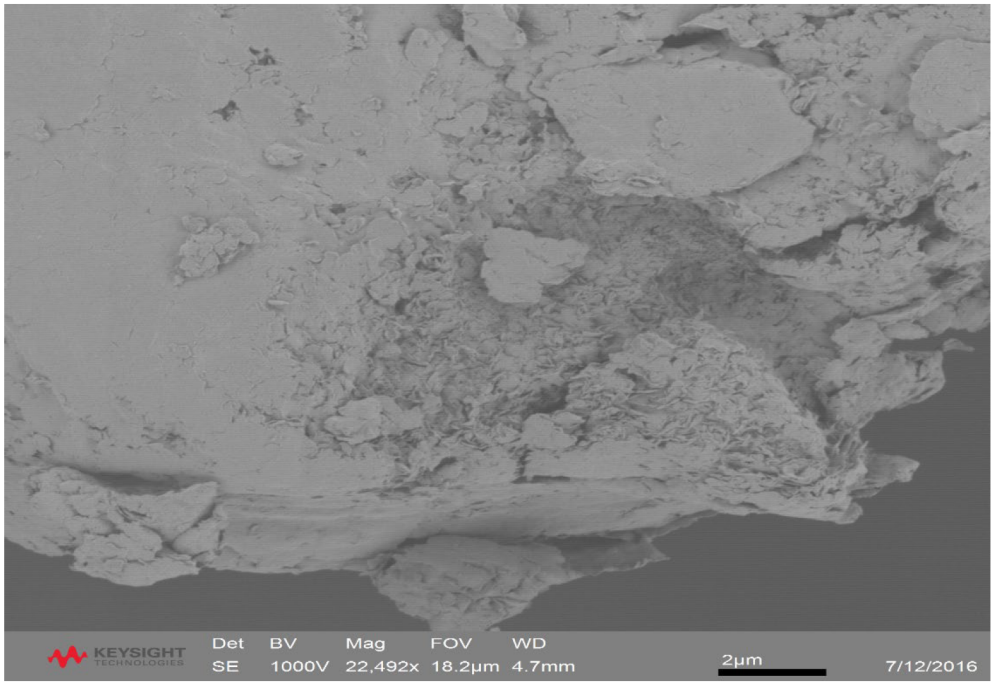

Figure 27b. LDH DS Persulfate using SEM at 22,492x

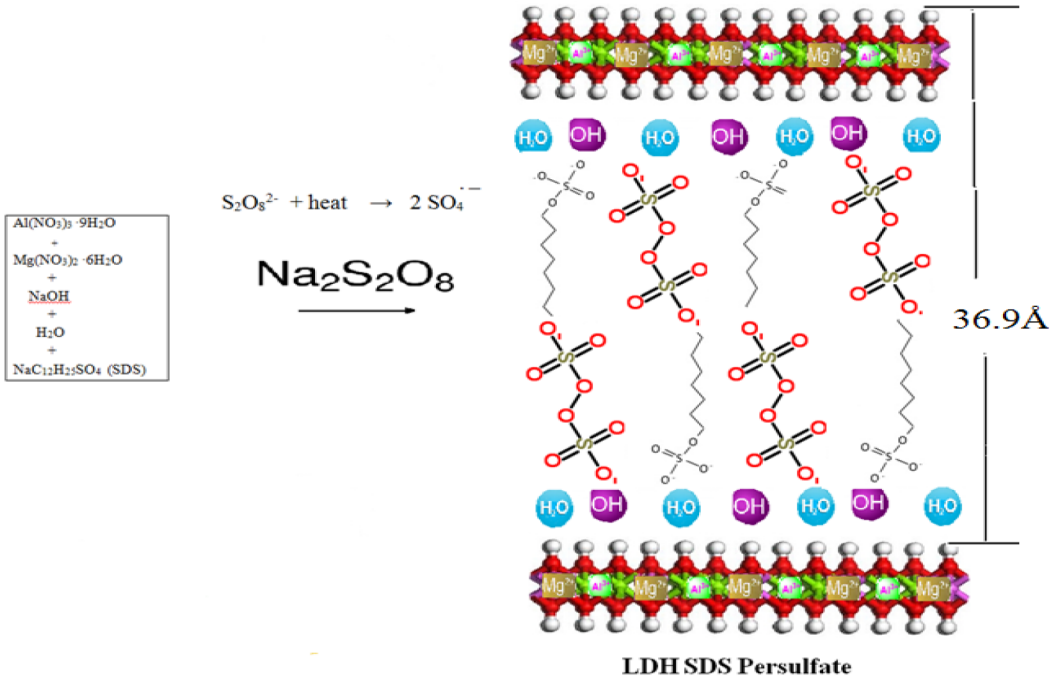

Figure 28. Schematic diagram of MgAl-LDH DS persulfate.

1.6 Conclusion

The need to identify counterfeit drugs effectively and inexpensively has a higher demand now than ever before, especially today in the 21st century, where the use of technology has advanced our knowledge and expanded our ideas. According to the World Health Organization (WHO), "almost half of the counterfeit drugs and low-quality drugs reported between 2013 and 2017, were found to be in sub-Saharan Africa".[1] The counterfeit drug market is wealthy generating, annually about $200 billion worldwide according to World Health Organization.[1] One of the significant reported reasons why the general public buys these drugs due to the high price for the brand name drugs that people could not afford, and they instead settle for the ones sold on the street.

The goal to develop an efficient and inexpensive means to identify molecules using imprinted polymers. There is a need for an inexpensive means of identifying and separating a specific molecule in the presence of a large number of other molecules. Preparation of designer polymers and carrying out polymerizations in well-controlled environments. The rationale for this project is that improved polymers prepared by carrying out the polymerizations in the customized environments of nanoscale mini reactors. The proposed mini reactors are the galleries of modified layered double hydroxides. The polymer matrix will have binding sites that have the shape and size that will bind the template used during the polymerization. The resulting polymer matrix will then recognize and bind to the target molecule. An additional requirement is that, if another -molecule placed into the polymer matrix, it will not fit into or bind to the

polymer matrix. We were successfully able to carry out Mg/Al-LDH-NO_3, Al/Mg-LDH-DS, Al/Mg-LDH-S_2O_8, and Al/Mg-LDH-DS/S_2O_8 in a well define the environment as illustrated in this dissertation. This new technique hopes to improve the synthesis and effectiveness of molecular imprinting in identifying specific molecules.

CHAPTER 2

QUANTUM EFFICIENCY OF CsSb PHOTOCATHODE

2.1 Introduction of Photocathode

At the early years by Gorlich (1936) who discovered that cesium antimonide holds a high quantum efficiency in the visible region (530nm), the compounds of antimony with the alkali metals have been the subject of significant research ever since.[84-86] Sommer (1958) has emerged this topic to the next level indicating that these antimonides have relatively low quantum efficiencies possess a hexagonal crystal structure. Whereas those antimonides such as Cs_3Sb, Na_2KSb, and $(Cs)Na_2LSb$, have quantum efficiencies greater than 10% possess a cubic crystal structure.[86]

Many types of photoemissive materials have been used as photocathodes to generate free electrons in practical applications. For example, robust metal photocathodes used in accelerator-based light sources, and low work function compound photocathodes used in photomultiplier tubes.[84-89] Photocathodes for electron accelerator applications such as energy recovery linacs (ERL) and free-electron lasers (FEL) operate with cesium transverse energy.[89] However, electron photo-excited from the cathode must be accelerated to relativistic velocities in the smallest possible distance to avoid the deleterious effects of space charge.[90] Among various photocathode materials, alkali antimonide such as K_3Sb, Cs_3Sb, K_2CsSb, and Na_2KSb have great promise in the

application of future light sources because of their high QE, fast response and low thermal emittance.[91-95]

Multi-alkali Multi-alkali antimonide photocathodes which are known to be excellent candidates for high-quality electron sources because of their quantum efficiency in the visible light range. Low emittance from these photocathodes surface is very useful for a lifetime, and fast response.[96] In general, an antimony layer is deposited onto the substrate as the first step, followed by potassium and then cesium deposition with an amount of material deposited controlled by maximizing the current from the photocathode in each Akali deposition step.[96]

The drive of this investigation was to explore the growth and spectral response of CsSb photocathode on Si, Al_2O_3, TiO_2, and SiC substrate along with their corresponding quantum efficiency. The thickness was measured using a quartz crystal microbalance (QCB). This study will give us a better understanding of CsSb and possible future substrates used to grow the CsSb photocathode.

2.2 Materials and Method

2.2.1 Technique used in Growing Photocathode

Table 12 shows the ultra-high vacuum schematic procedure for growing CsSb on multiple substrates. The deposition rate in respect to pressure, temperature (Cs and Sb), and flux vary for each measurement, and the measurement was measured using quartz micro-balance (QMB). The deposition growth for CsSb photocathode on Si, Al_2O_3, TiO_2, and SiC substrates illustrated in Table 12. The substrate was annealed between 5 hours to

6 hours with a heater current of 10A. The substrate was heated at high temperature to remove the hydrogen passivation from the Si surface and to clean any impurity from Al_2O_3, TiO_2, and SiC.[97] The thickness for each deposition varies, and each measurement obtained from the QMB. The stability of the Cs deposition determined the deposition of Sb during the growth.

Table 12. The Growth rates of Si, Al_2O_3, TiO_2, and SiC.

Substrate	Silicon (Si)	SiC	Al_2O_3	TiO_2
Pressure (base)	1.1e-9 Torr	1.8e-9 Torr	2.1e-9 Torr	2.46e-9 Torr
T(Cs)	65.8C	80.2C	81.3C	82.8C
T(Sb)	450C	460C	465C	463C
Flux (Cs)	3.5e12atoms/cm^2/s	7.5e12atoms/cm^2/s	1.1e13atoms/cm^2/s	9e12atoms/cm^2/s
Flux (Sb)	4e12atoms/cm^2/s	3.3e12atoms/cm^2/s	4.9e12atoms/cm^2/s	3e12atoms/cm^2/s
Thickness	7nm	10nm	16nm	5.5nm
QE	1.6%	6.2%	2.8%	3.3%

2.2.2 Sample Growth (CsSb on Si, Al_2O_3, TiO_2, and SiC)

The thin film growth performed in an ultra-high vacuum (UHV) equipped with turbopumps to ensure a base pressure in the low 1x10^{-10} Torr. Each substrate first degreased in acetone and isopropanol alcohol for 30mins and then etched in diluted aqueous hydrofluoric acid (HF) solution to remove the native oxide layer. After HF treatment, the substrate was rinsed with deionized water, dried under the stream of high purity nitrogen. Before the growth, the substrate was heated at 500°C under high vacuum

for further surface cleaning treatment. The CsSb photocathode film was produced by alternately introducing Cs and Sb vapor on Si, Al_2O_3, TiO_2, and SiC substrate. Cs and Sb generated by thermal evaporation. During the photocathode growth, the vapor deposition thickness and the photocathode response monitored with quartz crystal microbalance (QCM). First, Cs was evaporated onto Si and then exposed to Cs until the photocurrent reached a plateau before the evaporation of Sb. This process repeated for Al_2O_3, TiO_2, and SiC substrate in this work.

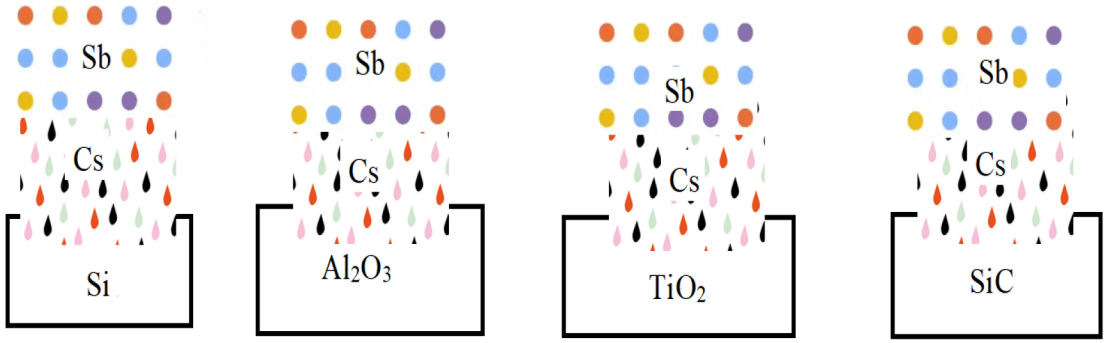

Figure 29. Schematic of Si, Al_2O_3, TiO_2, and SiC growth.

2.2.3 Vacuum Suitcase (for STM measurements)

One of the methods used to transport these photocathodes is suitcases, which avoid the exposure of air. The vacuum suitcase showed in Figure 30 consists of a magnetic translator arm connected to a small vacuum and a small ion pump. An all-metal gate valve used to isolate the suitcase containing cathode during the transfer from the deposition chamber where the photocathode growth took place to the load lock chamber

of the photoinjector gun. The photocathode transferred into this suitcase can then be characterized using the scanning tunneling microscope (STM).

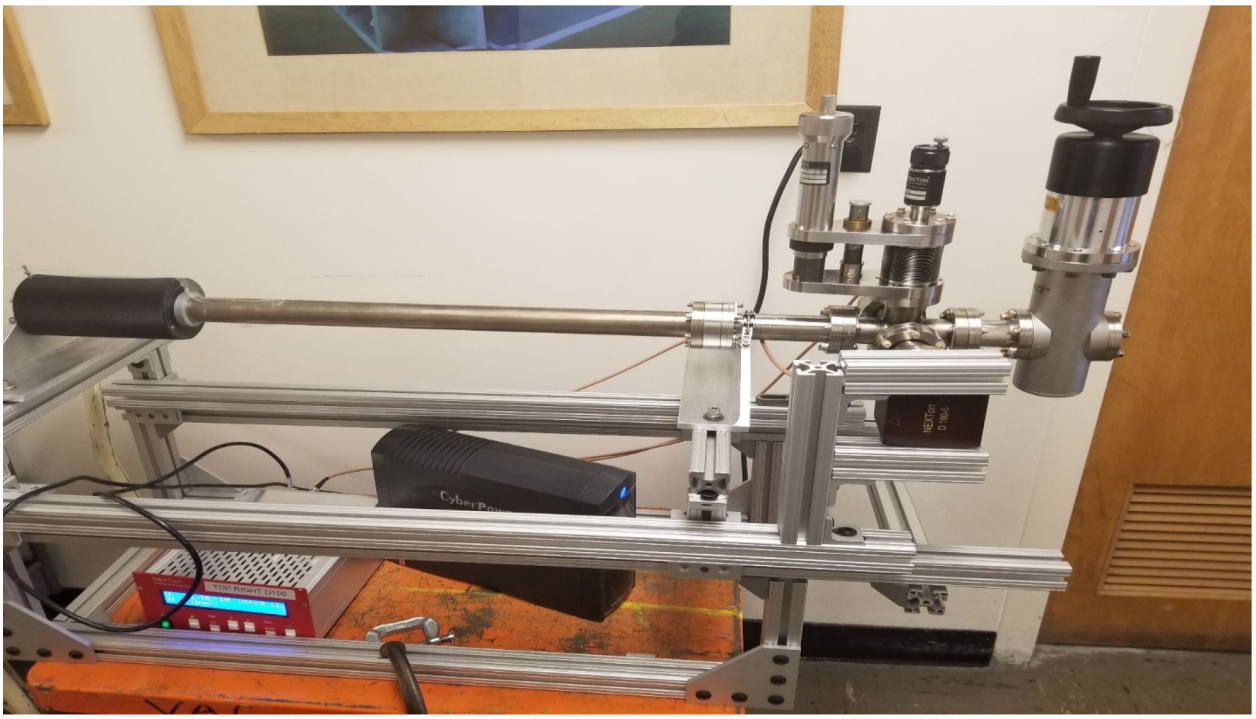

Figure 30. Vacuum suitcase.

2.3 Results and Discussion

2.3.1 CsSb on Si, Al_2O_3, TiO_2, and SiC Graphs

The laser sources used for measuring the QE value of the cathode grown are a small solid-state laser emitting 0.7 mW at 532.[97] The light power is measured using a power meter (Newport model 842-PE) coupled with a UV enhanced Silicon photodetector (Newport model 918D-UV-OD3).[97] During the thin film deposition, photoresponse recorded to monitor the film growth and the completion of the film deposition. A continue incident laser of 532nm wavelength generates a laser spot on the

surface of the photocathode obtained in Figure 31, Figure 32, and Figure 33. The QE calculated with equation 1:

$$QE = \frac{hcI_{ph}}{e\lambda P_0} \quad (1)$$

$$QE = \frac{1240 I_{ph}(A)}{\lambda(nm) P_0(W)} \times 100\%$$

Table 13: QE Values Calculated after Growth.

Substrate	Silicon (Si)	SiC	Al_2O_3	TiO_2
QE	0%	9.7%	2.8%	5.5%

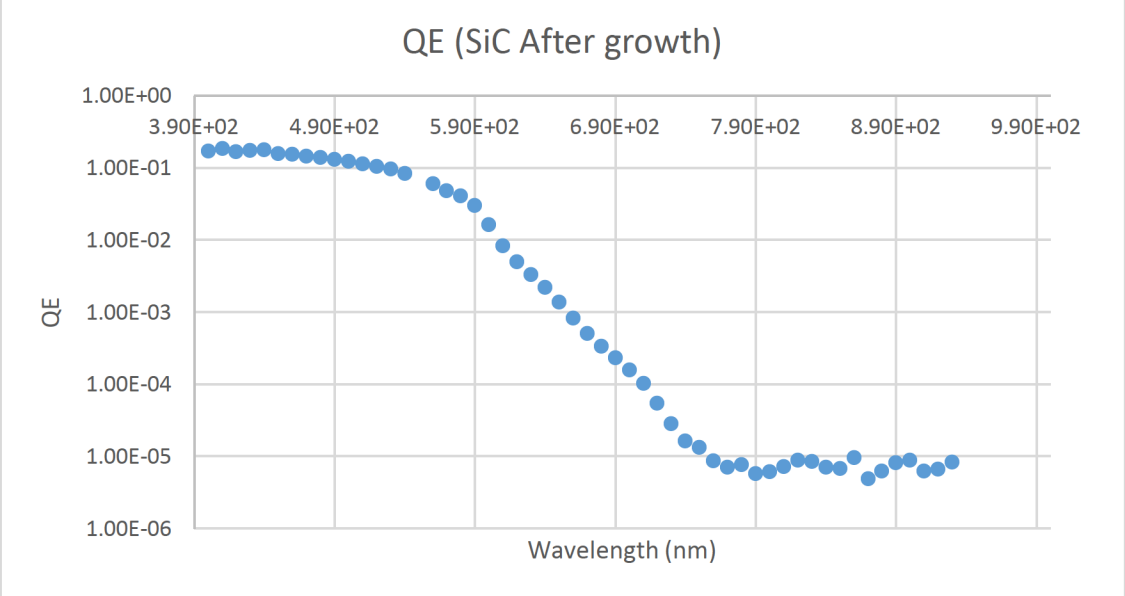

Figure 31. Graph of SiC plotted after growth.

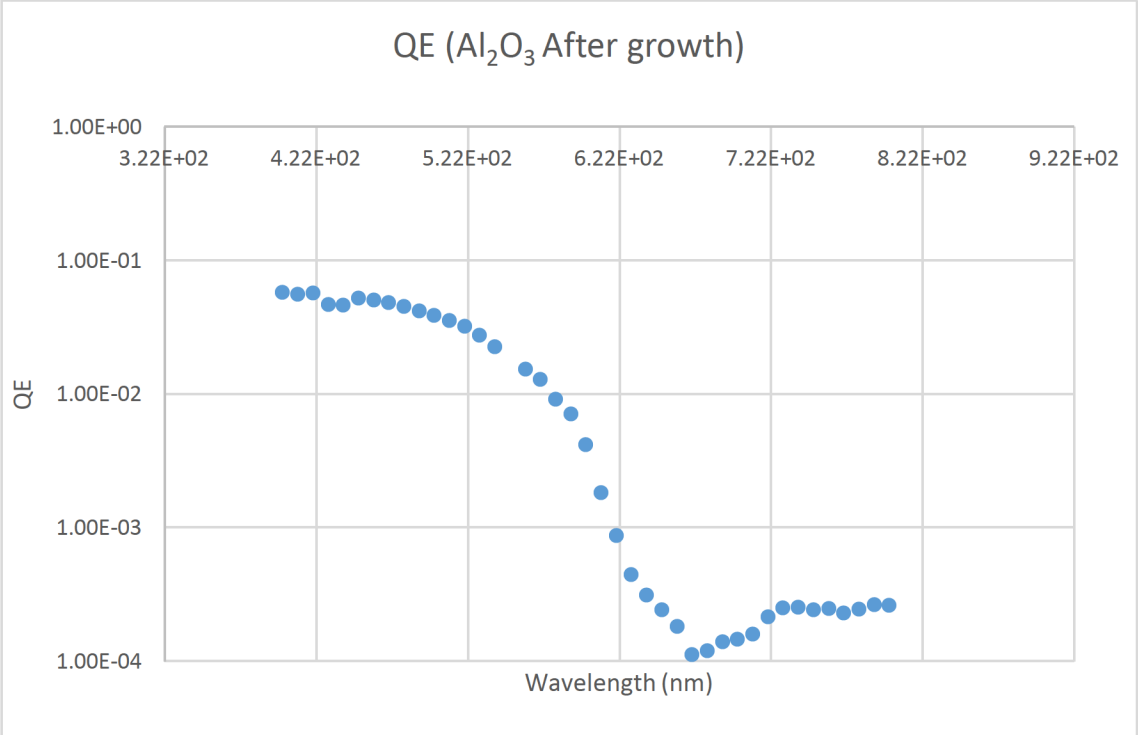

Figure 32. Graph of Al_2O_3 plotted after growth.

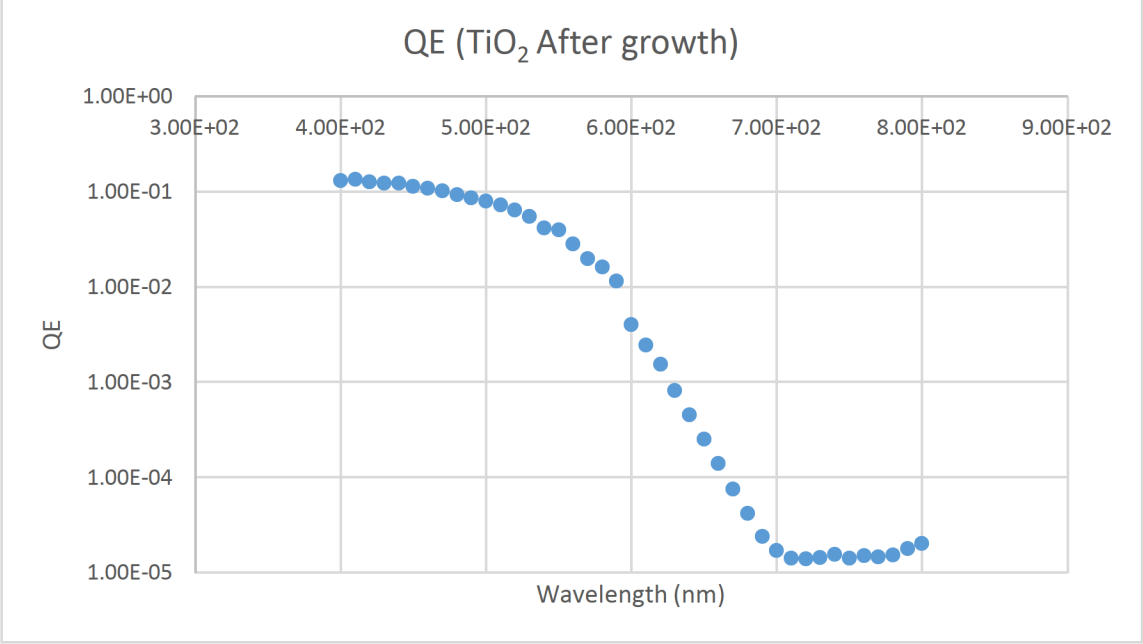

Figure 33. Graph of TiO_2 plotted after growth.

The spectral response of a typical CsSb photocathode grown on Si, SiC, Al_2O_3, and TiO_2 as described in the previous section shown in Table 1. The graph reports the QE value measured at 532 nm using a laser light source. The plot above demonstrates the Quantum efficiency versus photon wavelength measured in the 700-400 nm range. The QE value measure on Si, SiC, Al_2O_3, and TiO_2 at the laser wavelength are 0%, 9.7%, 2.8%, and 5.5%. As shown, CsSb photocathode grown on SiC reports the highest QE value, and this was a result of carbon. During the growth, carbon exposed to the chamber, which leads to a much promising result, discovered that carbon is essential for the uptake of having higher QE value.

2.4 Conclusion

Multi-alkali antimonide photocathodes which are known to be excellent candidates for high-quality electron sources because of their quantum efficiency in the visible light range. Low emittance from these photocathodes surface is very useful for a lifetime, and fast response.[96] In general, an antimony layer is deposited onto the substrate as the first step, followed by potassium and then cesium deposition with an amount of material deposited controlled by maximizing the current from the photocathode in each Akali deposition step.[96-98]

The drive of this investigation was to explore the growth and spectral response of CsSb photocathode on Si, Al_2O_3, TiO_2, and SiC substrate along with their corresponding quantum efficiency. The thickness was measured using a quartz crystal microbalance (QCB). During the growth, carbon exposed to the chamber, which leads to a much promising result, discovered that SiC is a better substrate for growth. The reason can be

that SiC forms a better interface with Cs_3Sb, probably because it does not contain oxygen. With an astonishing result, the promise of growing CsSb on a substrate containing carbon will expand and unlock the new phase of the photocathode. The conclusion from this investigation state that exposure to carbon was the key to obtaining a higher QE value.

REFERENCES

1. Christensen, S. "Tens of Thousands Die in Africa Each Year Due to Fake Drugs." *Reuters*, Thomson Reuters, 16 Nov. **2018**, https://www.reuters.com/article/us-westafrica-drugs-fake/tens-of-thousands-die-in-africa-each-year-due-to-fake-drugs-idUSKCN1NK23I.

2. Atabong, A.B. "African Healthcare Systems Are in an Arms Race with a Rising Fake Medicine Problem." *Quartz Africa*, Quartz, 22 Apr. **2019**, https://qz.com/africa/1601659/africas-counterfeit-drug-problem-being-tackled-by-innovators/.

3. Vasapollo, G.; Sole, D.R.; Mergola, L.; Lazzoi, R.M.; Scardino, A.; Scorrano, S.; Mele, G. Molecularly imprinted polymers: present and future prospective. *Int. J. Mol. Sci.* **2011**, *12*, 15908-5945.

4. Bossi, A.; Bonini, F.; Turner, F.; Piletsky, S.A. Molecularly imprinted polymers for the recognition of proteins: The state of the art. *Biosens Bioelectron*. **2007**, *22*, 1131–1137.

5. Chakraborty, J.; Roychowdhury, S.; Sengupta, S.; Ghosh, S. Mg-Al layered double hydroxide-methotrexate nanohybrid drug delivery system. *Materials and Science and Engineering*. **2013**, *33*, 2168-2174.

6. Costa, R.F.; Leuteritz, A.; Wagenknecht, U.; Jehnichen, D.; HauBler, L.; Heinrich, G. Intercalation of Mg-Al layered double hydroxide by anionic surfactants: preparation and characterization. *Applied clay science*. **2008**, *38*, 153-164.

7. Okutucu, B.; Onal, S. Molecularly imprinted polymers for separation of various sugars from human urine. *Talanta.* **2011**, *87*, 74-79.

8. Vasapollo, G.; Sole, D.R.; Mergola, L.; Lazzoi, R.M.; Scardino, A.; Scorrano, S.; Mele, G. Molecularly imprinted polymers: present and future prospective. *Int. J. Mol. Sci.* **2011**, *12*, 15908-5945.

9. Bi, X.; Zhang, H.; Dou, L. Layered double hydroxide-based nanocarriers for drug delivery. *Pharmaceutics*. **2014**, *6*, 298-332.

10. Piletsky, S.A.; Turner, N.W.; Laitenberger, P. Molecularly imprinted polymers in clinical diagnostics-future potential and existing problems. *Med. Eng. Phys.* **2006**, *28*, 971–977.

11. Li, W.; Li, S. Molecular imprinting: A versatile tool for separation, sensors, and catalysis. *Adv. Poly. Sci*. **2007**, *206*, 191–210.

12. Piletska, E.V.; Guerreiro, A.R.; Whitcombe, M.J.; Piletsky, S.A. Influence of the polymerization conditions on the performance of molecularly imprinted polymers. *Macromolecules*. **2009**, *42*, 4921–4928.

13. Morelli, I.; Chiono, V.; Vozzi, G.; Ciardelli, G.; Silvestri, D.; Giusti, P. Molecularly imprinted submicron spheres for applications in a novel model biosensor-film. *Sens. Actuators B*. **2010**, *150*, 394–401.

14. Longo, L.; Scorrano, S.; Vasapollo, G. RNA nucleoside recognition by phthalocyanine-based molecularly imprinted polymers. *J. Poly. Res*. **2010**, *17*, 683–687.

15. Shi, X.; Wu, A.; Qu, G.; Li, R.; Zhang, D. Development and characterizations of molecularly imprinted polymers based on methacrylic acid for selective recognition of drugs. *Biomaterials*. **2007**, *28*, 3741–3749.

16. Cavani, F.; TrifirÃ², F.; Vaccari, A. Hydrotalcite-type anionic clays: Preparation, properties and applications. *Catalysis Today*. **1991**, *11*, 173-301.

17. Tronto, J.; Bordonal, A.C.; Naal, Z.; Valim, J.B. Conducting polymers/ layered double hydroxides intercalated nanocomposites. *Open science, materials science.* **2013.**

18. Puoci, F.; Iemma, F.; Picci N. Stimuli-responsive molecularly imprinted polymers for drug delivery: A review. *Current Drug Delivery*. **2008**, *5*, 85–96.

19. Longo, L.; Vasapollo, G. Phthalocyanine-based molecularly imprinted polymers as nucleoside receptors. *Met-Based Drugs*. **2008**, 1–5.

20. Ge, Y.; Turner, F. Molecularly imprinted sorbent assays: Recent developments and applications. *Chem. Eur. J*. **2009**, *15*, 8100–8107.

21. Urraca, J.L.; Hall, A.J.; Moreno-Bondi, M.C.; Sellergren, B. A stoichiometric molecularly imprinted polymer for the class-selective recognition of antibiotics in aqueous media. *Angew Chem Int Ed*. **2006,** *45*, 5158–5161.

22. Nalawade, P.; Aware, B.; Kadam, J.V.; Hirlekar, S.R. Layered double hydroxides: A review. *Journal of Scientific & industrial research*. **2009**, *68*, 267-272.

23. Wulff, G.; Sarhan, A. Use of polymers with enzyme-analogous structures for the resolution of racemates. *Angew Chem. Int. Ed*. **1972**, *11*, 341–342.

24. Mosbach, K.; Ramström, O. The emerging technique of molecular imprinting and its future impact on biotechnology. *Nat Biotechnol*. **1996**, *14*, 163–170.

25. Sun, P.; Wang, Y.; Du, H.; Gu, T. Phosphate Removal and Recovery with Calcined Layered Double Hydroxides as an Adsorbent. *Phosphorus, Sulfur, and Silicon and the Related Elements.* **2008**, *183* (2-3), 519-526.

26. Khan, A.; O'Hare, D. Intercalation Chemistry of layered double hydroxides: recent developments and applications. *The Royal Society of Chemistry.* **2002**.

27. Bera, P.; Rajamathi, M.; Hegde, M.S.; Kamath, P.V. Thermal behavior of hydroxides, hydroxy salts and hydrotalcites. *Bull. Mater. Science*. **2000**, *23*, 141-145.

28. Manasse, E. Hydrotalcites as potential Catalyst for Hydroxylation of Phenol. *Att. Soc. Toscana Sci*. Nat., **1915**, 24, 92.

29. Fuda, K.; Sudo, N.; Kawai, S.; Matsunaga, T. Preparation of Zn/Ga-layered double hydroxide and its thermal decomposition behavior. *Chem. Lett*. **1993**, *22*, 777-780.

30. Thermal Analysis- TGA/DSC - Mooreanalytical. *https://www.mooreanalytical.com/thermal-analysis-tga-dsc/*. N.p., n.d. Web. July 13, **2019.**

31. Ruigrok, V.J.B.; Levisson, M.; Eppink, M.H.M.; Smidt, H.; Oost, J.V.D. Alternative affinity tools: more attractive than antibodies. *Biochemical Journal*. **2011**, *436*, 1-13.

32. Debecker, D. P.; Gaigneaux, E. M.; Busca, G. Exploring, Tuning, and Exploiting the Basicity of Hydrotalcites for Applications in Heterogeneous. *Catalysis. Chem. - A Eur. J.* **15**, 3920–3935 (**2009**).

33. Feitknecht, W.; Gerber, M. Double hydroxides and basic salts. Helv. Chim. *Acta*, **1942**, 25, 131.

34. Ruigrok, V.J.B.; Levisson, M.; Eppink, M.H.M.; Smidt, H.; Oost, J.V.D. Alternative affinity tools: more attractive than antibodies. *Biochemical Journal*. **2011**, *436*, 1-13.

35. Almojil, S.F.; Othman, M.A. Screening Different Divalent and Trivalent Metals Containing Binary and Ternary Layered Double Hydroxides for Optimum Phosphate Uptake. *Sci Rep* **9,** 15511 (**2019**) doi:10.1038/s41598-019-52031-w

36. Li, R. *et al*. Enhancing phosphate adsorption by Mg/Al layered double hydroxide functionalized biochar with different Mg/Al ratios. *Sci. Total Environ.* **559**, 121–129 (**2016**).

37. Bernardo, M. P.; Moreira, F. K.V.; Colnago, L. A; Ribeiro, C. Physico-chemical assessment of [Mg-Al-PO4]-LDHs obtained by structural reconstruction in high concentration of phosphate. *Colloids Surfaces A Physicochem. Eng. Asp.* 497, 53–62 (**2016**).

38. Everaert, M. *et al*. Phosphate-Exchanged Mg-Al Layered Double Hydroxides: A New Slow Release Phosphate Fertilizer. *ACS Sustain. Chem. Eng.* **4**, 4280–4287 (**2016**).

39. Khitous, M.; Salem, Z.; Halliche, D. Removal of phosphate from industrial wastewater using uncalcined MgAl-NO $_3$ layered double hydroxide: batch study and modeling. *Desalin. Water Treat.* **57**, 15920–15931 (**2016**).

40. Cheng, X.; Wang, Y.; Sun, Z.; Sun, D.; Wang, A. Pathways of phosphate uptake from aqueous solution by ZnAl layered double hydroxides. *Water Sci. Technol*. **67** (**2013**).

41. Novillo, C. *et al*. Evaluation of phosphate removal capacity of Mg/Al layered double hydroxides from aqueous solutions. *Fuel* 138, 72–79 (**2014**).

42. Mills, J.S.; Christy, G.A.; Genin, M.J.; Kameda, T.; Colombo, F. Nomenclature of the hydrotalcite supergropup natiral layered double hydroxides. *Mineralogical magazine*. Oct. **2012**. Vol. 76(5), pp. 1289-1336.

43. Ladewig, K.; Xu, A.P.; Lu, G.Q. Potential for Layered Double Hydroxide-Based Innovative Drug Delivery System. Expert Opin. *Drug Deliv*., 6 (**2009**), pp. 907-922.

44. Omwoma, S.; Chen, W.; Tsunashima, R.; Song Coord, Y.F; Environmentally benign polyoxometalate materials. *Chem. Rev*., 258–259 (**2014**), pp. 58-71.

45. Yokoi, T.; Tsukada, K.; Terasaka, S.; Kamitakahara, M.; Matsubara, H. Morphological control of layered double hydroxide through a biometric approach using carboxylic and sulfonic acid. *Journal of Asian Ceramic Societies*. Volume 3, Issue 3, **2015**, pp 230-233.

46. Feitknecht, W.; Gerber, M. Double hydroxide and basic salts. Helv. Chim. *Acta*, **1942**, 25, 131.

47. Miyata, S. Physico-chemical properties of synthetic hydrotalcites in relation to composition. *Clays Clay Miner*. **1980**, *28*, 50-56.

48. Xu, Z.; Yoon, G.; Park, K.; Park, H.; Tamwattana, O.; Kim, S.; Seong, W.M.; Kang, K. Tailoring sodium intercalation in graphite for high energy and power. Nature Communications. Article number: 2598 (**2019**).

49. Song, H.; Fukutsuka, T.; Miyazaki, K.; Abe, T. Superssion of co-intercalation reaction of propylene carbonate and lithium ion into graphite negative electrode by addition of diglyme. Journal of the Electerochemical Society. **2016**. Vol. 163, issue 7, A1265-A1269.

50. Tronto, J.; Bordonal, A.C.; Naal, Z.; Valim, J.B. Conducting Polymers / Layered Double Hydroxides Intercalated Nanocomposites, Materials Science - Advanced Topics. *Mast. Intech Open*. **2013**. DOI: 10.5772/54803.

51. Sarac, A.S. Rodox polymerization. *Progress in Polymer Science*. 24. (**1999**) 1149-1204.

52. Lv, W.; Mei, Q.; Du, M.; Xiao, J.; Ye, W.; Zheng, Q. Interaction between poly(vinyl alcohol) and Layered Double Hydroxide (LDH) particles with different topological shape and their application in electronspinning. *The Journal of Physical Chemistry*. **2016**. 120 (26). Pp. 14435-14443.

53. Tronto, J.; Bordonal, A.C.; Naal, Z.; Valim, J.B. Conducting polymers/ layered double hydroxides intercalated nanocomposites. *Open science, materials science.* **2013.**

54. Chalasani, R.; Gupta, A.; Vasudevan, S. Engineering new layered solids from exfoliated inorganics: a periodically alternating hydrotalcite-montmorillonite layered double hydroxide. *Science report*. **2001.** Vol. 3. Pp. 3498.

55. Matsui, J.; Kato, T.; Takeuchi, T.; Suzuki, M.; Yokoyama, K.; Tamiya, E.; Karube, I. Molecular recognition in continuous polymer rods prepared by a molecular imprinting technique. *Anal Chem***. 1993.** *65*, 2223–2225**.**

56. Nalawade, P.; Aware, B.; Kadam, J.V.; Hirlekar, S.R. Layered double hydroxides: A review. *Journal of Scientific & industrial research*. **2009***, 68*, 267-272.

57. Crescenzi, C.; Bayoudh, S.; Cormack, P.A.; Klein, T.; Ensing, K. Determination of clenbuterol in bovine liver by combining matrix solid-phase dispersion and molecular imprinted solid-phase extraction followed by liquid chromatography/electrospray ion trap multiple-stage mass spectrometry. *Anal Chem*. **2001**, *73*, 2171–2177.

58. Kempe, M.; Mosbach, K. Separation of amino acids, peptides and proteins on molecularly imprinted stationary phases. *Journal Chromatogram A*. **1995**, *691*, 317–323.

59. Yan, S.; Fang, Y.; Gao, Z. Quartz crystal microbalance for the determination of daminozide using molecularly imprinted polymers as recognition element. *Biosens Bioelectron*. **2007**, *22*, 1087–1091.

60. Greenwell, C.H.; Jones, W.; Rugen-Hankey, L.S.; Holliman, J.P.; Thompson, L.R. Efficient synthesis of ordered organo-layered double hydroxides. *Green Chem*. **2010**, *12*, 688-695.

61. Caro, E.; Marce, R.M.; Sherrington, D.C.; Borrull, F. A new molecularly imprinted polymer for the selective extraction of naproxen from urine samples by solid-phase extraction. *J Chromatogram B*. **2004**, *813*, 137–143.

62. Kempe, M.; Mosbach, K. Direct resolution of naproxen on a noncovalently molecularly imprinted chiral stationary-phase. *Journal Chromatogram A*. **1994**, *664*, 276–279.

63. Piletsky, S.A.; Andersson, H.S.; Nicholls, I.A. Combined hydrophobic and electrostatic interaction-based recognition in molecularly imprinted polymers. *Macromolecules*. **1999**, *32*, 633–636.

64. Karlsson, B.C.G.; O'Mahony, J.; Karlsson, J.G.; Bengtsson, H.; Eriksson, L.A.; Nicholls, I.A. Structure and dynamics of monomer-template complexation: An explanation for molecularly imprinted polymer recognition site heterogeneity. *J. Am. Chem. Soc*. **2009**, *131*, 13297–13304.

65. Hart, B.R.; Shea, K.J. Synthetic peptide receptors: Molecularly imprinted polymers for the recognition of peptides using peptide-metal interactions. *Journal Am Chem Soc*. **2001**, *123*, 2072–2073.

66. Scorrano, S.; Longo, L.; Vasapollo, G. Molecularly imprinted polymer for solid-phase extraction of 1-methyladenosine from human urine. *Anal Chim Acta*. **2010**, *659*, 167–171.

67. Prasad, B.B.; Tiwari, K.; Singh, M.; Sharma, P.S.; Patel, A.K.; Srivastava, S. Molecularly imprinted polymer-based solid-phase microextraction fiber coupled with molecularly imprinted polymer-based sensor for ultra-trace analysis of ascorbic acid. *Journal Chromatogram A*. **2008**, *1198*, 59–66.

68. Shi, X.; Wu, A.; Qu, G.; Li, R.; Zhang, D. Development and characterizations of molecularly imprinted polymers based on methacrylic acid for selective recognition of drugs. *Biomaterials*. **2007**, *28*, 3741–3749.

69. Javanbakht, M.; Shaabani, N.; Abdouss, M.; Ganjali, M.R.; Mohammadi, A.; Norouzi, P. Molecularly imprinted polymer for selective solid-phase extraction of verapamil from biological fluids and human urine. *Current Pharm Anal*. **2009**, *5*, 269–276.

70. Masqué, N.; Marcé, R.M.; Borrull, F.; Cormack, G.; Sherrington, D.C. Synthesis and evaluation of a molecularly imprinted polymer for selective on-line solid-phase extraction of 4-nitrophenol from environmental water. *Anal Chem*. **2000**, *72*, 4122–4126.

71. Sellergren, B. Direct drug determination by selective sample enrichment on an imprinted polymer. *Anal Chem*. **1994**, *66*, 1578–1582.

72. He, C.; Long, Y.; Pan, J.; Li, K.; Liu, F. Application of molecularly imprinted polymers to solid-phase extraction of analytes from real samples. *Journal Biochem. Biophys. Meth*. **2007**, *70*, 133–150.

73. Turiel, E.; Martin-Esteban, A. Molecularly imprinted polymers for sample preparation: *Review Anal Chim. Acta*. **2010**, *668*, 87–99.

74. Del Sole, R.; Scardino, A.; Lazzoi, M.R.; Vasapollo, G. Molecularly imprinted polymer for solid phase extraction of nicotinamide in pork liver samples. *Journal Appl. Polym. Sci*. **2011**, *120*, 1634–1641.

75. Javanbakht, M.; Attaran, A.M.; Namjumanesh, M.H.; Esfandyari-Manesh, M.; Akbari-adergani, B. Solid-phase extraction of tramadol from plasma and urine samples using a novel water-compatible molecularly imprinted polymer. *Journal Chromatogram B*. **2010**, *878*, 1700–1706.

76. Del Sole, R.; Lazzoi, M.R.; Arnone, M.; Della Sala, F.; Cannoletta, D.; Vasapollo, G. Experimental and computational studies on non-covalent imprinted microspheres as recognition system for nicotinamide. *Molecules*. **2009**, *14*, 2632–2649.

77. Yañez, F.; Chianella, I.; Piletsky, S.A.; Concheiro, A.; Alvarez-Lorenzo, C. Computational modeling and molecular imprinting for the development of acrylic polymers with high affinity for bile salts. *Anal Chim. Acta*. **2010**, *659*, 178–185.

78. Pietrzyk, A.; Kutner, W.; Chitta, R.; Zandler, M.E.; D'Souza, F.; Sannicolò, F.; Mussini, P.R. Melamine acoustic chemosensor based on molecularly imprinted polymer film. *Anal Chem*. **2009**, *81*, 10061–10070.

79. O'Mahony, J.; Karlsson, G.; Mizaikoff, B.; Nicholls, I.A. Correlated theoretical, spectroscopic, and X-ray crystallographic studies of a non-covalent molecularly imprinted polymerization system. *Analyst*. **2007**, *132*, 1161–1168.

80. Chakraborty, J.; Roychowdhury, S.; Sengupta, S.; Ghosh, S. Mg-Al layered double hydroxide-methotrexate nano-hydride drug delivery system: Evaluation of efficacy. *Materials Science and Engineering*. **2013**, C33, 2168-7174.

81. Longo, L.; Scorrano, S.; Vasapollo, G. RNA nucleoside recognition by phthalocyanine-based molecularly imprinted polymers. *J. Polym. Res.* **2010**, *17*, 683–687.

82. Wulff, G.; Sarhan, A. Use of polymers with enzyme-analogous structures for the resolution of racemates. *Angew. Chem. Int. Ed.* **1972**, *11*, 341–342.

83. *Oxidation of Alcohols*, www.chemguide.co.uk/organicprops/alcohols/oxidation.html.

84. Arshady, R.; Mosbach, K. Synthesis of substrate-selective polymers by host-guest polymerization. *Macromol. Chem. Phys.* **1981**, *182*, 687–692.

85. Kon, S.H.; Kinross-Wright, J.; Nguyen, D.C.; Sheffield, R.L. *Nucl. Instrum. Methods Phys. Res*. **1995**, A 358, 272.

86. Yang, J.; Sakai, F.; Yanagida, T.; Yorozu, M.; Okada, Y.; Takasago, K.; Endo, A.; Yada, A.; Washio, M. *J. Appl. Phys*. **2002**, 92, 1608.

87. Wang, X.J.; Rao, T.S.; Batchelor, K.; Ben-Zvi, I.; Fischer, J. *Nucl. Instrum. Methods Phys. Res.* A 356, 159.

88. Moszynski, M.; Gierlik, M.; Kapusta, M.; Nassalski, A.; Szczesniak, T.; Fontaine, C.; Lavoute, P. *Nucl. Instrum. Methods Phys. Res*. **2006**, A 567, 31.

89. Kume, H.; Suzuki, S.; Takeuchi, J.; Oba, K. *IEEE Trans. Nucl. Sci*. **1985**, 32, 448.

90. Spicer, W.E. *Appl. Phys*. **1977**, 12, 115.

91. Child, C.D. *Appl. Phys*. **1911**, 32, 492.

92. Van Oerle, B.M.; Ernst, G.J. *Nucl. Instrum. Methods Phys. Res*. **1995**, A 358, 287.

93. Bazarov, I.V.; Cultrera, L.; Bartnik, A.; Dunham, B.; Karkare, S.; Li, Y.; Xianghong, X.; Maxson, J.; Roussel, W. *Appl. Phys. Lett*. **2011**, 98, 224101.

94. Cultera, L.; Karkare, S.; Lillard, B.; Bartnik, A.; Bazarov, I.; Dunham, B.; Schaff, W.; Smolenski, K. *Appl. Phys. Let.* **2013**, 103, 103504.

95. Vecchione, T.; Ben-Zvi, I.; Dowell, D.H.; Feng, J.; Rao, T.; Smedley, J.; Wan, W.; Padmore, H.A.; *Appl. Phys. Lett.* **2011**, 99, 034103.

96. Cultrera, L.; Karkare, S.; Bartnik, A.; Bazarov, I.; Dunham, B.; Merluzzi, R.; Nichols M. *Appl. Phys. Let.* **2011**, 99, 152110.

97. Sommer, A.H. *Photoemissive Materials: Preparation, Properties, and Use*. *John Wiley & Sons Inc*., **1969.**

98. Cultrera, L.; Bazarov, I.V.; Conway, J.V.; Dunham, B.; Karkare, S.; Li, Y.; Liu, X.; Maxson, J.M.; Smolenski, W. *Growth and characterization of bialkali photocathodes for Cornell ERL injector*. Particle Accelerator Conference. **2011**